COMMISSIONING OF HIGH SPEED IMAGING SYSTEM FOR RAINBOW SCHLIEREN MEASUREMENTS OF VAPORIZING LIQUID FUEL SPRAYS

by

EILEEN MARIE MIRYNOWSKI

JOSHUA A. BITTLE, COMMITTEE CHAIR
AJAY K. AGRAWAL
ALEXEY N. VOLKOV
CHIH-HSIUNG CHENG

A THESIS

Submitted in partial fulfillment of the requirements
for the degree of Master of Science
in the Department of Mechanical Engineering
in the Graduate School of
The University of Alabama

TUSCALOOSA, ALABAMA

2016

ABSTRACT

The fuel injection process has been studied since the internal combustion engine was developed. Direct injection has been an integral part to the success of diesel engines, where there is minimal time for the fuel to mix with the compressed air. The benefits of fuel injection center on: fuel efficiency and lower toxic emissions. As the world depletes more fossil fuels each year it is imperative to concentrate research on techniques to lower fuel consumption. Past research on fuel sprays using laser techniques were limited by cross sensitivity in regards to the regions with both liquid and vapor phases present. Quantitative schlieren techniques have been proposed and investigated since the first half of the 20th century, but only recently with the rapid development of digital imaging techniques and computers have they have been used for quantitative analysis.

This thesis presents the results for a new hardware installation for a rainbow schlieren diagnostic method. Experiments were performed using a constant pressure flow vessel (CPFV) and a modern common rail diesel injector to obtain high-speed images of the vaporizing fuel sprays. The CPFV ran under steady ambient thermodynamic conditions where the pressure and temperatures were controlled variables. Two cameras were used, Mie scatter liquid phase data and the rainbow schlieren vapor phase data were captured simultaneously. Quantitative results indicate that the axial and radial variation in the fuel sprays seem to match the well-validated variable profile model.

LIST OF ABBREVIATIONS AND SYMBOLS

3D	three-dimensional
CPFV	constant pressure flow vessel
SADI	stand-alone direct injector
CDAQ	control and data acquisition system
LED	light emitting diode
LTC	low-temperature combustion
TDC	top dead center
PCCI	premixed charge compression ignition
HCCI	homogeneous charge compression ignition
PM	particle matter
RGB	red, green and blue
RSD	rainbow schlieren deflectometry
HSB	hue, saturation and brightness
LIF	laser-induced fluorescence
LIEF	laser induced exciplex fluorescence
EPA	environmental protection agency

ACKNOWLEDGMENTS

Having the opportunity to pursue my Masters degree at the University of Alabama has been an incredible experience, one that I will never forget. It would not have been possible without help from my amazing support system of family and friends. There were so many people that encouraged and prayed for me along the way. Dad, Mom, Kelley, Cole, Eddie and to the rest of my family and friends, thank you for helping me persist through the stressful times and celebrating with me during the good times. I want to thank my advisor, Dr. Joshua Bittle, and my committee members, Dr. Agrawal, Dr. Volkov and Dr. Cheng, for all of their time and support. I especially want to express my gratitude to Dr. Bittle for taking me on as a graduate research assistant. One of my greatest blessings has been having him as my mentor. I would not have made it without all of his help and guidance over the past few years.

Although my time as a student at the University of Alabama has come to an end, I will take the pride of this school with me where ever I go. I will never forget the influential people I met or the lessons I learned along the way. Roll Tide.

CONTENTS

ABSTRACT ii

LIST OF ABBREVIATIONS AND SYMBOLS iii

ACKNOWLEDGMENTS iv

LIST OF TABLES vii

LIST OF FIGURES viii

1. INTRODUCTION 1

1.1 Motivation 1

1.2 Previous Work 2

1.3 Low-Temperature Combustion 6

1.4 Schlieren Imaging Background 8

1.5 Previous Rainbow Schlieren Work 12

2. EXPERIMENTAL SETUP 13

2.1 Constant Pressure Flow Vessel 13

2.2 Rainbow Schlieren Setup 15

2.3 Filter Selection 17

2.4 Software 19

3. RESULTS AND DISCUSSION 31

4. SUMMARY, CONCLUSION AND FUTURE WORK 40

REFERENCES 42

APPENDIX A. MATLAB CODES 44

APPENDIX B. HUE CALIBRATION GRAPHS 52

LIST OF TABLES

2.2 High-speed imaging optics and cameras.....16

2.3 Deflection angles of the symmetric filters used in this experiment 18

LIST OF FIGURES

Figure 1.1 Conventional diesel engine.....2

Figure 1.2.1 Mie scattering versus Rayleigh scattering.....4

Figure 1.2.2 Musculus and Kattke's variable profile model.....5

Figure 1.2.3 Model predictions and Rayleigh-scatter results 6

Figure 1.3.1 Illustration of low temperature combustion (LTC) and the corresponding levels of NOx and soot emissions 7

Figure 1.3.2 Illustration of low temperature combustion (LTC) and corresponding levels of CO and other hydrocarbon emissions 8

Figure 1.4.1 Schematic diagram of a monochrome schlieren setup using a knife-edge 9

Figure 1.4.2 Schlieren image of high and low sensitivity.....9

Figure 1.4.3 Schematic diagram of a lens-type rainbow schlieren setup.10

Figure 1.4.4 Comparison of symmetrical verses non-symmetrical filters 11

Figure 2.1.1 Constant pressure flow vessel (CPFV) illustration 14

Figure 2.1.2 Isometric view of CPFV 14

Figure 2.2.1 Overhead view of optics and CPFV 16

Figure 2.3.1 Images of the three filters used with the smaller aperture for this experiment 17

Figure 2.3.2 Images of the four filters used with the larger aperture for this experiment 17

Figure 2.4.1 Filter calibration for hue versus the distance on the filter from previous work 19

Figure 2.4.2 Hue calibration graph for 2.5 mm symmetric filter.....21

Figure 2.4.3 Mirrored hue calibration graph for 2.5 mm symmetric filter 21

Figure 2.4.4 Snapshot of a single injection using the 1.25mm filter at frame 16 using small aperture 22

Figure 2.4.5 Snapshot at frame 16 of the average code for 50 injections using the 0.75 mm filter 23

Figure 2.4.6 Snapshot at frame 16 of the average code for 50 injections using the 1.25 mm filter 23

Figure 2.4.7 Snapshot at frame 16 of the average code for 50 injections using the 1.75 mm filter 24

Figure 2.4.8 Mie-scatter liquid boundary overlaid with the footage taken from the Phantom v611.....26

Figure 2.4.9 Comparison of frames from a single injection with frames from the 50 injections averaged together using the 2.5mm symmetrical filter 27

Figure 2.4.10 Radial characterization using a 1.75mm symmetric filter...29

Figure 2.4.11 Radial characterization at 180°C using a 2.5 mm symmetric filter 30

Figure 3.1 Comparison of 0.75mm, 1.25mm and 1.75mm symmetrical filters at 200°C 32

Figure 3.2 Comparison of the radial characterization between the four filters at 180°C 35

Figure 3.3 Comparison of the radial characterization of varying temperatures using the 2.5mm symmetric filter 37

1. INTRODUCTION

1.1 Motivation

Understanding of the fuel injection processes can enable better combustion control and lead to more accurate predictions resulting in a reduction of fuel consumption and toxic emissions. Diesel engines are being widely incorporated due to their efficiency over that of a traditional gasoline engine. One of the main differences between a gasoline and diesel engine is how the fuel air mixture is ignited. In a typical gasoline engine air and fuel are mixed together, compressed by the pistons then ignited by a spark delivered from the spark plugs. The ignition of the fuel and air mixture forces the piston downward and the process begins again. A diesel engine injects the fuel into a chamber of already compressed air. When air is compressed it heats up, the fuel reacts with the compressed heated air and ignites. This process allows a diesel engine to have a higher compression ratio over a gasoline engine. A gasoline engine compression ratio can go from 8:1 to 12:1, while a diesel engine compression ratio can go from 14:1 to 25:1. A higher compression ratio will increase the thermal efficiency, which will in turn lead to more power and also lead to a more lean operation. A conventional diesel engine diagram is illustrated in Figure 1.1.

There are some drawbacks; diesel engines cannot use three-way catalyst like a traditional gasoline engine so there are elevated levels of hydrocarbons and carbon monoxide (CO) emissions. Recent studies are taking a closer look at what is happening inside the combustion chamber. The goal is centered on how to develop a system that is more fuel efficient, while also reducing toxic emissions. Specifically when studying the fuel spray, many of the current

methods researchers are using to investigate the transient liquid fuel sprays are limited by cross sensitivity when studying regions with both liquid and vapor phases present (i.e. upstream of the liquid length). The quantitative rainbow schlieren deflectometry (RSD) technique has been demonstrated in the past for gaseous fuel jets and is being developed here to measure the density gradients in the fuel spray. Due to the lack of cross sensitivity issues, RSD enables measurement of the equivalence ratio throughout the spray.

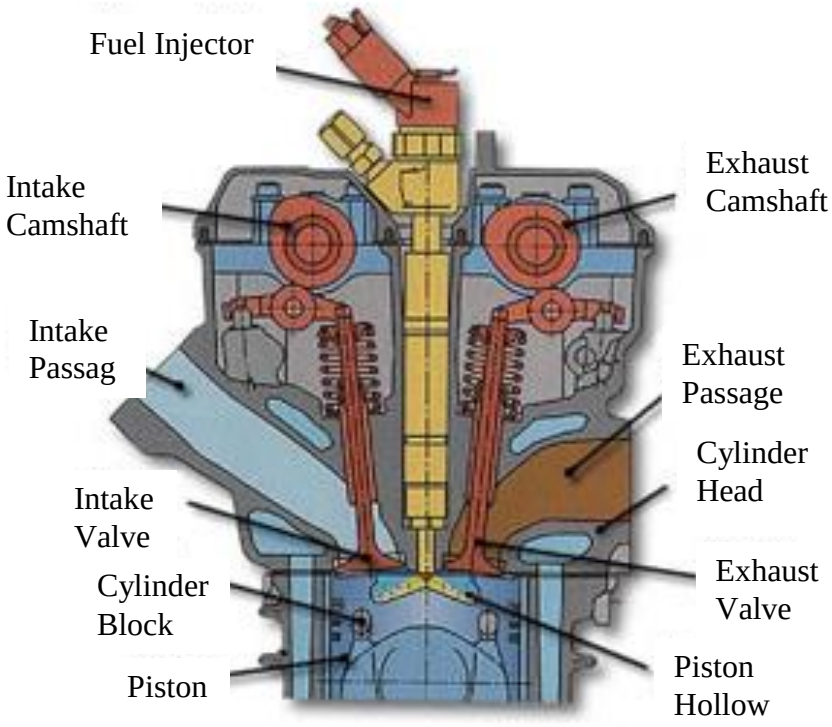

Figure 1.1 Conventional diesel engine [1].

1.2 Previous Work.

Compression ignition engines typically operate as heterogeneous combustion systems whereby the processes of fuel injection, atomization, vaporization, mixing with the cylinder air mixture, and then combustion are extremely complex. Siebers was able to show that for

injections into the high-density, high-temperature environment (i.e. near the peak compression conditions for an engine) the injected liquid fuel behaved very predictably according to his model [2]. That study was the culmination of many different experiments in an optically accessible spray chamber. Following the predictable injection behavior, Dec conceptually described combustion under typical conditions as a steady mixing-controlled flame once injection and combustion had stabilized [3]. Essentially the initially fuel rich core of the injection is mixed with ambient air and transported toward a standing flame surrounding the fuel/air plume. This discussion was aided and verified with optical diagnostic techniques. As engine technology has changed over the past two decades – with a trend towards using more in-cylinder combustion diagnostics and control techniques to minimize emissions and increase efficiency – these models have not adequately explained observations made under newly developed advanced combustion modes.

Some of these newer diagnostics include Raman scattering, Laser-induced fluorescence / exciplex fluorescence (LIF/LIEF), Mie scattering and Rayleigh scattering. There are advantages and setbacks to the processes listed above. Raman scattering uses energy to scatter photons, or inelastic scattering. This process is limited due to low signal intensity. LIF/LIEF incorporates an exciplex tracer to enhance the ability of detecting both the liquid and vapor phase of the fuel spray at various wavelengths. However, quantifiable data has only been achievable for the vapor phase of the spray. The Mie-scatter technique adds a tracer to the fuel to show the liquid phase of the fuel spray. Common diagnostic tools measure the magnitude and angle of liquid and vapor penetration. Achieving quantitative data is limited due to boiling point of the added tracer [4-6]. Picket et al. used Rayleigh scatter imaging to validate the fuel mixing predictions of new spray/mixing models proposed by Musculus and Kattke [7-8]. This method uses elastically

scattered incident light directly from the fuel molecules, so no fuel tracer is needed and the amount of scattered light is proportional to the mole fraction of the species present [9]. Knowing the ambient gaseous composition, the difference caused by the fuel presence can be quantified. Rayleigh scattering measurements have the disadvantage of being sensitive to interference from laser scattering sources other than the species of interest. This is particularly a problem near the injector were significant liquid fuel is still present and would cause interference. Picket et al. addressed this issue by only probing downstream of the maximum liquid length; this compromise however misses some potentially important information. Figure 1.2.1 below shows a comparison between the Mie scattering and Rayleigh scattering techniques.

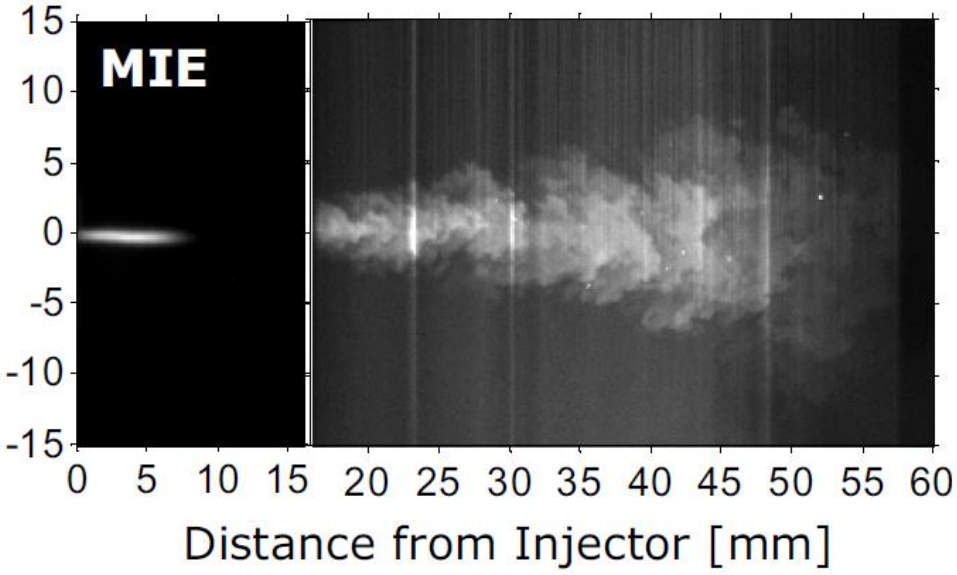

Figure 1.2.1 Mie scattering versus Rayleigh scattering [9].

The left side of the figure is a Mie scattering image that captures the liquid phase of the spray near the injector. The right side is a Rayleigh scattering image that captures the vapor phase of the spray downstream of the injector. As previously mentioned, in the Mie scattering image there is no definition between what is the vapor phase verses the liquid phase of the fuel

injection. The Rayleigh scattering image shows some of the smaller density gradients around the edge of the spray and the intensity of the light is proportional to the amount of fuel vapor. Musculus and Kattke were able to utilize the uniform-profile non-vaporizing model by Naber and Siebers to develop the variable profile model, which simulates mixing characteristics of a spray. This model is shown in Figure 1.2.2. The density profile defines the relationship expected as the fuel spray moves downstream. The density level peaks in the center of the spray, where the liquid phase is present. As the spray expands outward sufficient mixing / vaporization occurs and the density level goes down.

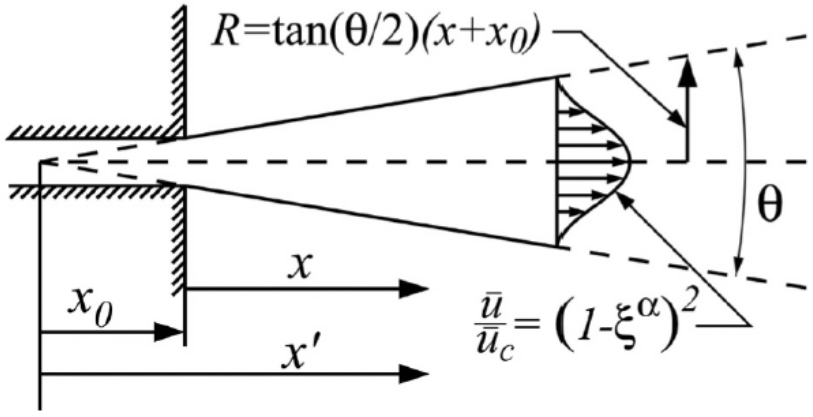

Figure 1.2.2 Musculus and Kattke's variable profile model [8].

Figure 1.2.3 was used in comparison with research pertaining to the Rayleigh-scatter method. The correlation between the centerline mixture fraction versus the axial distance was determined through the variable profile model. The correlation between the mixture fraction and the radial distance, or the results from the Rayleigh-scatter method, were then determined. The purpose of these graphs was to be able to show if the variable profile model is comparable to the experimental results. The model predictions are shown in the red lines and the experimental data are shown in the solid blue lines. The data achieved by the Rayleigh-scatter method does

successfully compare to the variable profile model predictions in most of the graphs achieved through this particular experiment.

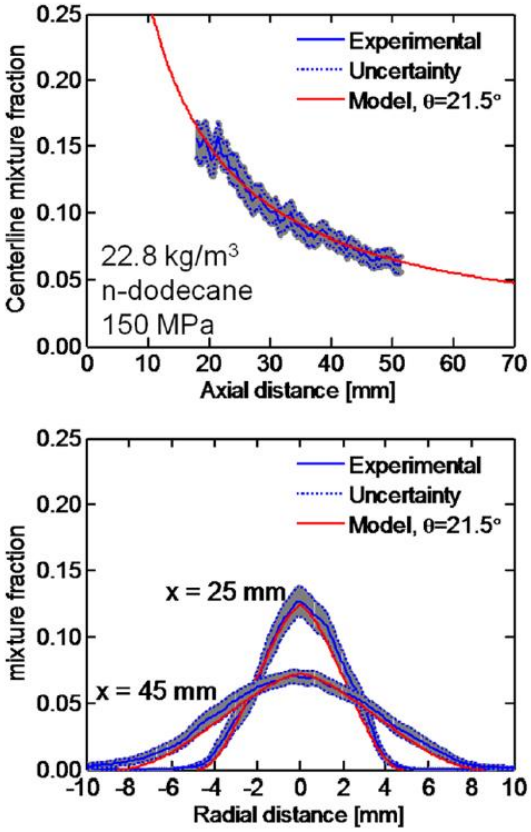

Figure 1.2.3 Model predictions (top) and Rayleigh-scatter results (bottom) [10].

1.3 Low-Temperature Combustion

Due to the increase Environmental Protection Agency (EPA) and Clean Air Act regulations of greenhouse gas emissions there is a need to develop more fuel efficient processes. There is an ever increasing growth in the amount of cars and trucks on the road each year that heightens the need for fuel efficiency to be a top priority. These regulations' primary goal is to reduce NOx, CO_2 and PM emissions. Research has developed and incorporated diesel engines that are successful in meeting these regulations. Thought to be two of the more advanced processes developed were the Homogeneous Charge Compression Ignition (HCCI) and

Premixed Charge Compression Ignition (PCCI). These processes ultimately can be described as Low-Temperature Combustion (LTC). Many of the new diagnostic and modeling tools have been developed to study these LTC operating conditions.

As the name describes, LTC uses lower temperatures to achieve combustion with the goal of lowering NOx emissions. In one aspect this is an advantage because at a lower temperature the NOx chemistry is altered and ultimately reduced as well as the soot produced [11-12]. Fuel is that is rich will have a higher soot formation, while fuel that is combusted under rising temperatures will have higher NOx emissions. The goal is to develop a system that will use leaner fuel and lower temperatures to achieve combustion.

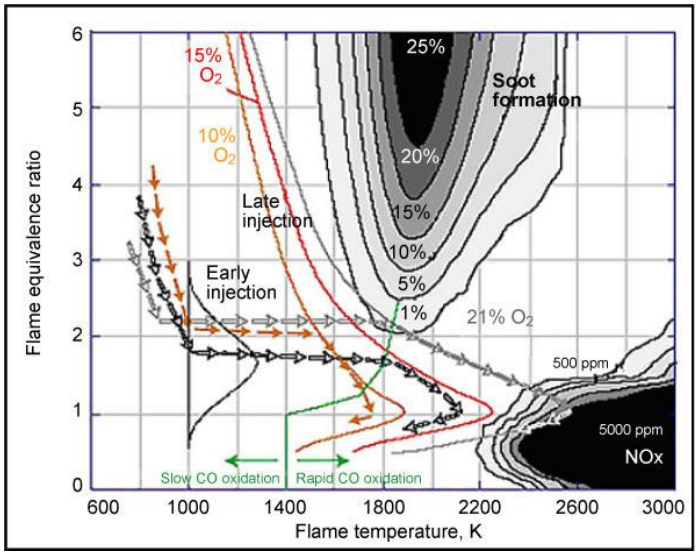

Figure 1.3.1 Illustration of low temperature combustion (LTC) and the corresponding levels of NOx and soot emissions [12].

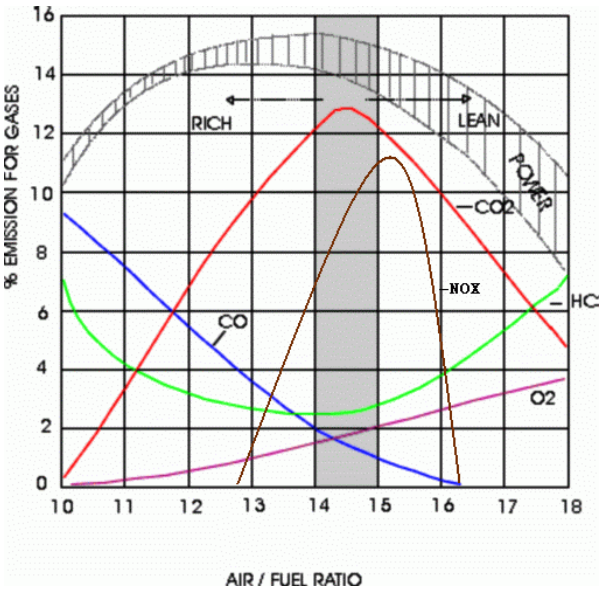

Figure 1.3.2 Illustration of low temperature combustion (LTC) and corresponding levels of CO and other hydrocarbon emissions [13].

However, a disadvantage is the increase of CO and unburned hydrocarbon emissions released. This concept is illustrated in Figure 1.3.2. The rise of CO and hydrocarbons counteract the efficiency of the diesel engine. The push to move forward with diesel engines is the having more power and lowering toxic emissions.

1.4 Schlieren Imaging Background

More recent research, by Panigrahi, utilized a monochrome schlieren technique, which incorporates a knife-edge to control the amount of light penetration [14]. This technique is illustrated in Figure 1.4.1. The amount of light penetration correlates to the capture of the varying density gradients throughout the fuel spray.

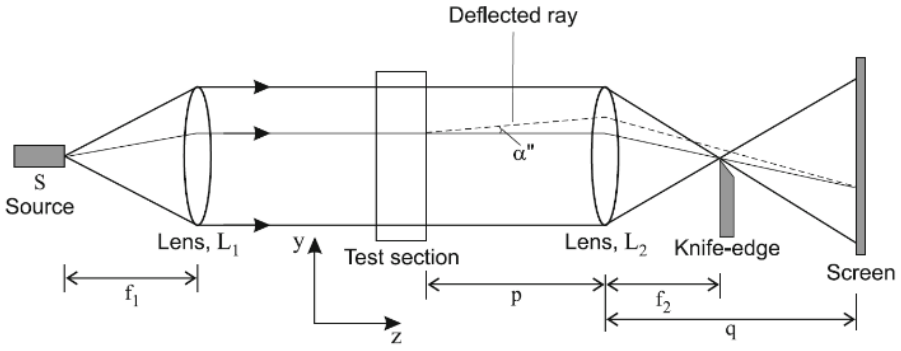

Figure 1.4.1 Schematic diagram of a monochrome schlieren setup using a knife-edge [14].

Figure 1.4.2 shows higher verses lower sensitivity, the vapor boundary is shown in green. By decreasing the amount of light, raising the knife-edge higher, there was a higher sensitivity. While increasing the amount of light, lowering the knife-edge, there was a lower sensitivity. The spray length and angle are tangible, but there is no way to differentiate between which is the liquid phase or vapor phase of the spray. Another disadvantage is that the background density gradients cannot be made out clearly requiring an image subtraction to highlight the vapor boundary.

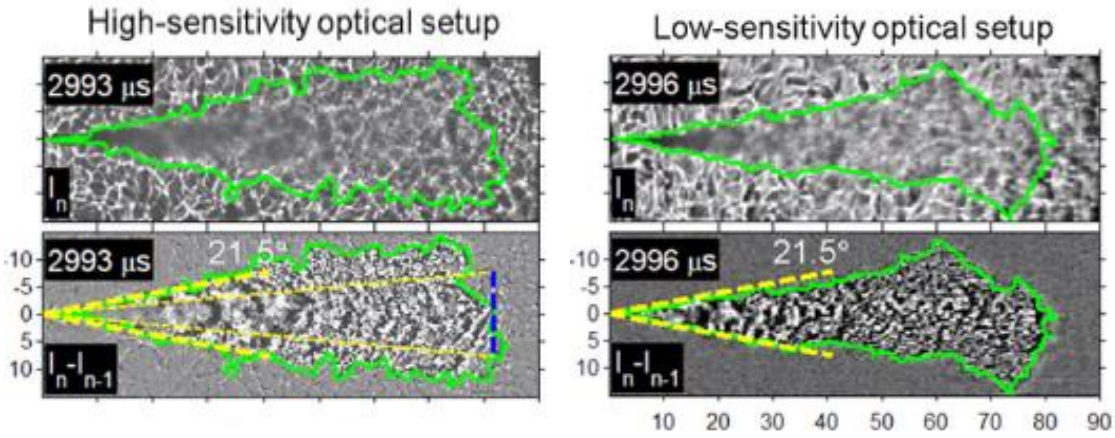

Figure 1.4.2 Schlieren image of high and low sensitivity [10].

Focus moved to incorporating a gray scale filter in place of the knife edge, which was able to show the angle of deflection. This morphed into the utilization of a colored filter and replacing the laser with an LED light source. This setup is illustrated in Figure 1.4.3**.**

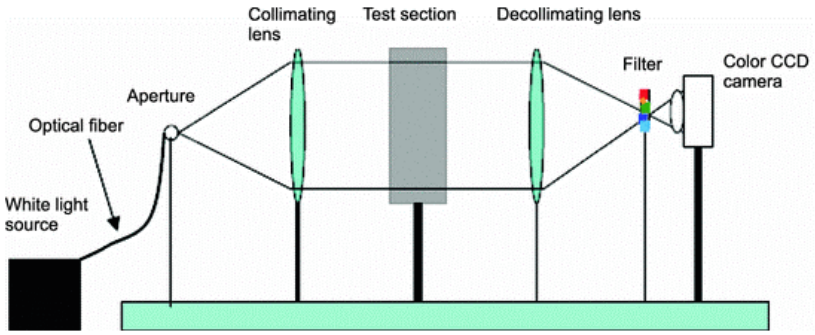

Figure 1.4.3 Schematic diagram of a lens-type rainbow schlieren setup [13].

The principle of rainbow schlieren setup is identical to that of the monochrome schlieren technique in that density gradients are mapped into light beam deflection. The rainbow filter measures the light displacement, and shows this displacement through an array of colors. The schlieren setup is aligned in the axial direction, which means the filter is sensitive to light displacement in the transverse direction. Two different types of filters were tested, symmetrical and non-symmetrical. The symmetrical filter varies on the Violet, Indigo, Blue, Green, Yellow, Orang, Red (VIBGYOR) scale so that the center color is red and the outer edges of the filter are violet on the top and bottom. The non-symmetrical filter varies on the same scale, but begins with violet and ends with red. Figure 1.4.4 shows a symmetrical verses non-symmetrical filter.

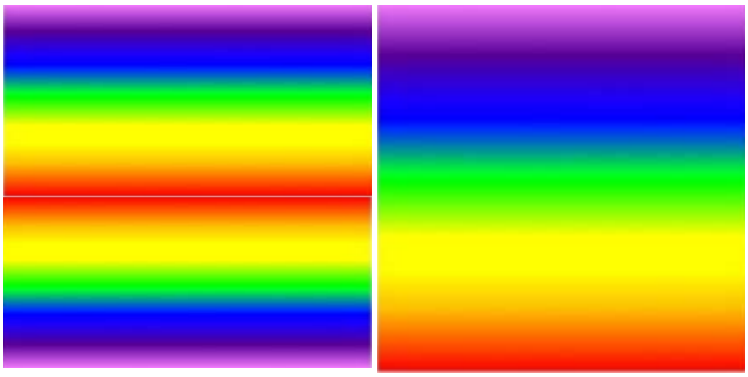

Figure 1.4.4 Comparison of symmetrical verses non-symmetrical filters [15].

On the left is an example of a symmetrical filter (using the VIBGYOR scale). The image on the right is an example of a non-symmetrical filter (using the VIBGYOR scale) [15]. As light penetrates the spray, some of the light will get deflected proportionally to the density gradients in the fluid it passes through. This light then passes through the color filter taking on a color which determines the angle of deflection, which will determine the density gradient. The maximum deflection distance capable of being detected by a given filter is determined by dividing the size of the filter by two. The maximum deflection angle is determined by finding the tangent angle between the focal length and the deflection distance. This experiment utilized symmetrical filters that ranged in sizes from 0.75 mm, 1.0 mm, 1.25 mm, 1.75 mm, 2.0 mm, 2.5 mm and 5.0 mm. Experimental data was also taken using two different apertures, referred to as the small aperture and large aperture, dimensions given in Table 2.2.1. The amount of light penetration was studied through the two different size apertures used. A smaller aperture would let less light penetrate through to the filter so smaller filters were applied. While the larger aperture let through more light, a wider range of aperture sizes were applied. The symmetric filters that were used with the smaller aperture were 0.75 mm, 1.25 mm and 1.75 mm. The symmetric filters that were used with the larger aperture were 1.0 mm, 2.0 mm, 2.5 mm and 5.0 mm.

1.5 Previous Rainbow Schlieren Work

The work of the others described above represents some of the current state of the art in experimental liquid fuel spray visualization techniques. There are other methods but all suffer from similar limitations. The work begun here has the ability to address those limitations and advance our understanding of the critically important fuel/air mixing process relevant to nearly all liquid fuel burning systems. Understanding this concept will lead to bridging the gap between higher fuel efficiency and lower toxic emissions.

The rainbow schlieren technique has been applied in a number of gaseous phase experiments by other members of the authors institution for quantitative measurements in a helium jet, temperature distributions in 3D heated air jets, temperature and oxygen concentrations in hydrogen jet diffusion flames, temperature measurements in flickering diffusion flames, and density measurements in supersonic microjet. The original schlieren setup incorporated a knife-edge to control the amount of light absorption. There were a few areas that suffered limitations. These limits included the inadequate absorption and nonlinearities in the medium [16-19]. A gray scale was developed and resulted in quantitative measurements. From there color coding schlieren technique was developed by Settles. There were limitations with these filters, the sensitivity was dependent on the number of colors on the filter and the spatial resolution was dependent on the discontinuities where the color boundaries were located. Howes developed a color filter that had a continuous color spectrum. Greenberg et al. used these filters in quantitative measurements in a Rainbow Schlieren Deflectometry (RSD) technique [20]. The primary motivation for applying this technique to the liquid fuel sprays is because of the insensitivity to liquid phase in the imaging window. This is contrary to traditional laser based techniques, which must be tuned for conditions without liquid fuel present.

2. EXPERIMENTAL SETUP

2.1 Constant Pressure Flow Vessel

In order to visualize the diesel-like fuel sprays at elevated temperatures and pressures under non-reacting conditions a constant pressure flow vessel (CPFV) is used as shown in Figures 2.1.1-2. The CPFV is capable of running at pressures up to 1380 kpa (200 psi) and temperatures up to 200°C. Although these values are less than that of maximum compression engine conditions, it enables effective advanced low-temperature combustion experiments where existing models are not validated. The sweep gas from the compressor passes through a heater before it enters the chamber through diffusion plates to generate a uniform flow. It is expected, and verified in the high-speed schlieren videos that the bulk gas motion/momentum is effectively zero compared to the fuel injection velocity. This type of configuration allows for rapid repetition of experimental conditions to quickly acquire large statistically significant data sets (i.e. many injections per minute) compared to traditional constant volume spray visualization chambers. More details on the design and construction of the CPFV can be found in [5].

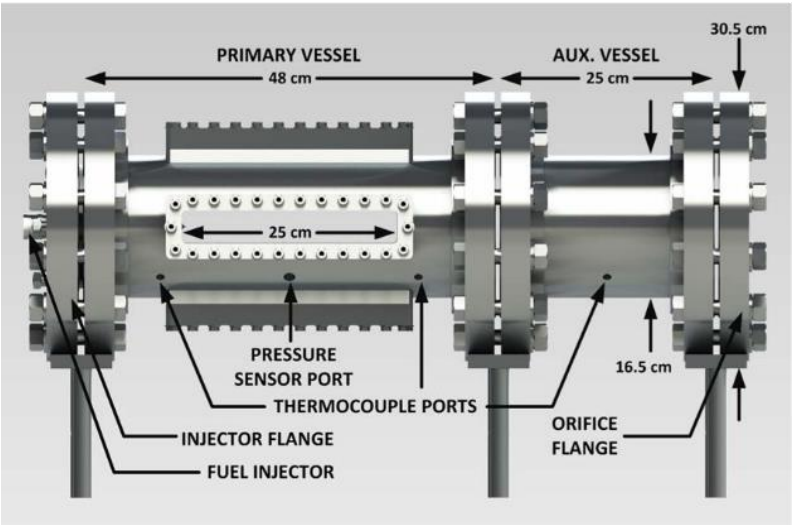

Figure 2.1.1 Constant pressure flow vessel (CPFV) illustration [21].

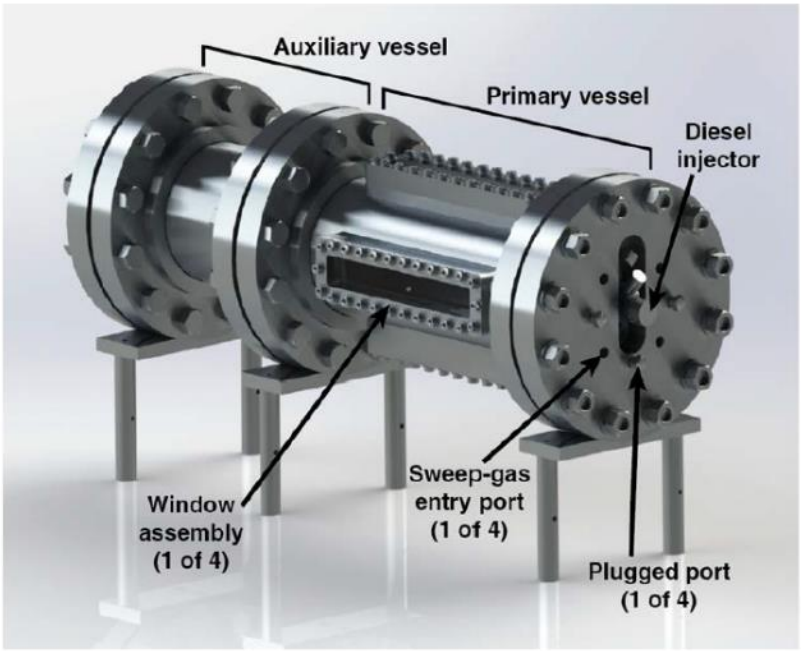

Figure 2.1.2 Isometric view of CPFV [21].

The diesel injector used is a Bosch CRIN3 solenoid driven common-rail injector capable of up to 180 MPa injection pressures. The injector was modified to have a single hole (100 μm) at the tip to spray a fuel jet axially down the center of the CPFV windows. An electronic stand-alone direct injector (SADI) driver controls the injector. A LabVIEW program was created to

control the driver, which provides the high current electrical signal that drives the solenoid and actuates the injector. The fuel cart supplies high pressure fuel (n-heptane in this case) to the injector using an air driven pressure multiplier which is suitable for injection rates on the order of one per second as is the case for the CPFV. A control and data acquisition (CDAQ) system was used to obtain experimental data. The CDAQ controlled the trigger timing of the injector and the spray visualization cameras and lights.

A coolant system was incorporated to enable more control over the temperature of the injector. Throughout this experiment the temperature was set at 90˚C to simulate engine coolant temperatures.

2.2 Rainbow Schlieren Setup

The schlieren setup includes a laser driven plasma light source (LDLS) coupled to a fiber optic cable to produce high intensity broadband light. This is passed through an aperture mounted at the focal point of a collimating lens. The distance from the collimating lens to the aperture needed to be set so there was a three inch diameter (size of lens) beam of light exiting the lens (too close and the beam will diverge, too far and it will converge). The parallel beam is passed through the windows in the primary vessel of the CPFV illuminating the injector tip and the spray. The light is then collected by a de-collimating lens and passes through a printed color filter strip placed at the imaging plane of the lens. The location of the colored filter was set to capture the apex of the light that traveled through the de-collimating lens. Details about the filter selection is in section 2.3. The light then enters the camera, which is mounted close enough to capture entire schlieren image and is focused on the mid-plane of the spray. The size of the lenses (3 inches) restricts the field of view to approximately 70 mm downstream of the injector. All of the components were set up on stands attached to a track to ensure axial alignment. The

liquid phase is imaged separately using Mie-scattering techniques from an orthogonally mounted pulsed generated laser driven plasma light source (LDLS) mounted in the top window. This system generates and intense sheet of light approximately 3mm thick towards the fuel spray in-sync with the camera framing rate. The setup is shown in Figure 2.2.1. The cameras, light sources and other optics are summarized in Table 2.2.

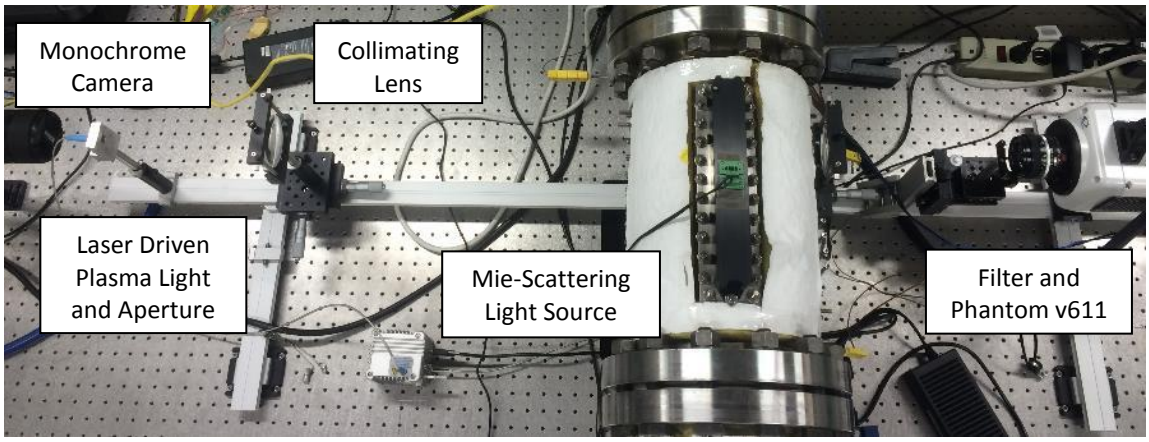

Figure 2.2.1 Overhead view of optics and CPFV.

Rainbow schlieren equipment	
Light source	Energetiq Laser Driven Light Source (LDLS)
Small aperture dimensions	5 μm by 3 mm
Large aperture dimensions	100 μm by 3 mm
Achromatic collimating lens	3 in (76.2mm), focal length 250 mm
Colored filter size	1 mm, 1.75 mm, 2.5 mm and 5 mm
Color filter spectrum (symmetric)	320°- 40°-320° Hue
Color camera for schlieren images	Phantom v611
Mie-scattering imaging equipment	
Monochrome camera	Vision Research Phantom v7.3
Light source	Lightspeed Technologies, HPLS-36DD7500

Table 2.2 High-speed imaging optics and cameras.

The refractive index gradients in the test-section appear as colors in the schlieren image. The colors in the image represent angular deflection of light rays by the test media. In addition to providing quantitative measurements of deflection angle across the whole field, the rainbow

schlieren technique requires only a low power incoherent light source and it is less sensitive to optical misalignments.

2.3 Filter Selection

Due to light deflection the filter size and symmetric makeup were vital components to this experiment. Many filter sizes with symmetrical and non-symmetrical makeup were tested. It was determined that seven of these filters would be used with two different aperture sizes to collect the data for this thesis. The filters were symmetrical and the sizes were 0.75mm, 1mm, 1.25mm, 1.75mm, 2mm, 2.5mm and 5mm. The color bands are printed on standard projector film slides. The filters are shown in Figures 2.3.1-2.

Figure 2.3.1 Images of the three filters used with the smaller aperture for this experiment.

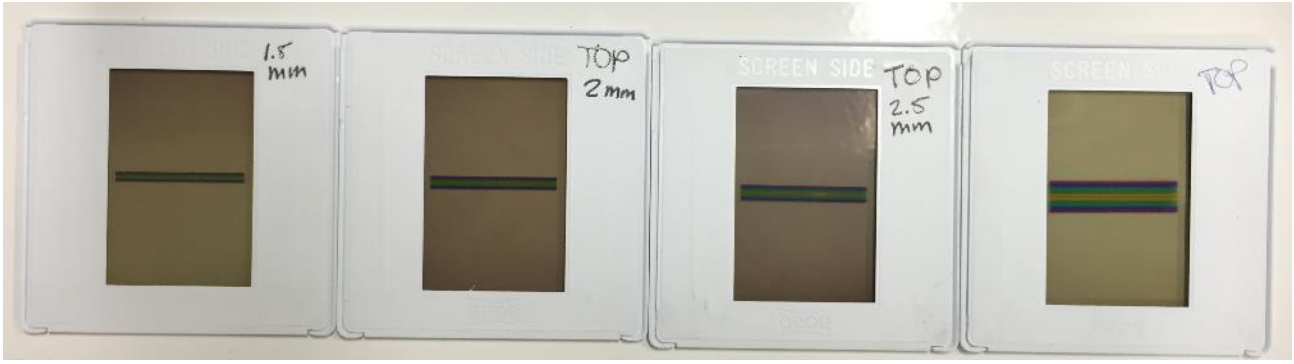

Figure 2.3.2 Images of the four filters used with the larger aperture for this experiment.

The first step was to have the correct white balance set. As you can note from above the background film on the filters varies in darkness. This was done by aligning the filter so the

LDLS light shown through a clear portion of the film. By right clicking on the image there was an option to open up the white balance. After determining that white balance for all three filters a calibration test was performed. Snap shot pictures were taken in 0.1mm intervals for each filter. These pictures were entered through a code on Matlab that generated a graph of hue vs location. Then a video was captured for 50 injections with a 90 μm exposure time, for two locations. The locations were set at the injector tip and further downstream. Each video was ran through a code that averaged the 50 injections in an ensemble average so that the result was a uniform axisymmetric spray clearly depicting the varying colors. The maximum deflection distance was calculated for each filter by dividing the filter size by two. The maximum deflection angle (in radians) was calculated by finding the tangent of the deflection distance divided by the focal length of 250mm which is approximated as Equation 1 below.

$$\epsilon = \frac{\Delta x}{f} \tag{1}$$

The deflection distance and maximum deflection angle for the filters are shown in Table 2.3 below.

Filter Size (mm)	Deflection Distance (mm)	Max Deflection Angle (degree)
0.75	0.375	0.08
1	0.5	0.11
1.25	0.625	0.14
1.75	0.875	0.20
2	1	0.23
2.5	1.25	0.28
5	2.5	0.57

Table 2.3 Deflection angles of the symmetric filters used in this experiment.

2.4 Software

As previously stated, a LabVIEW based control and data acquisition (CDAQ) program was used to monitor the varying temperatures and pressures across the CPFV as well as provide the trigger for the fuel injections [5]. There were four temperature ports that were studied along with one pressure port. Temperature 1 and 2 were from the thermocouple ports and the pressure was taken from the pressure sensor port shown in Figure 2.1.1. The upstream flange temperature was captured by putting a thermocouple in between the flanges on the left side of the chamber.

The videos were captured with a PCC 2.6 computer program that received data from the Phantom v611 for RSD data as well as the Phantom v7.3 for Mie scatter data. The data collected was ran through four main codes on MATLAB. A code was designed to calibrate the filters and to give a hue versus displacement location graph and a condensed hue verses displacement graph. Previous experiments described how to accurately acquire the data for filter calibration [14].

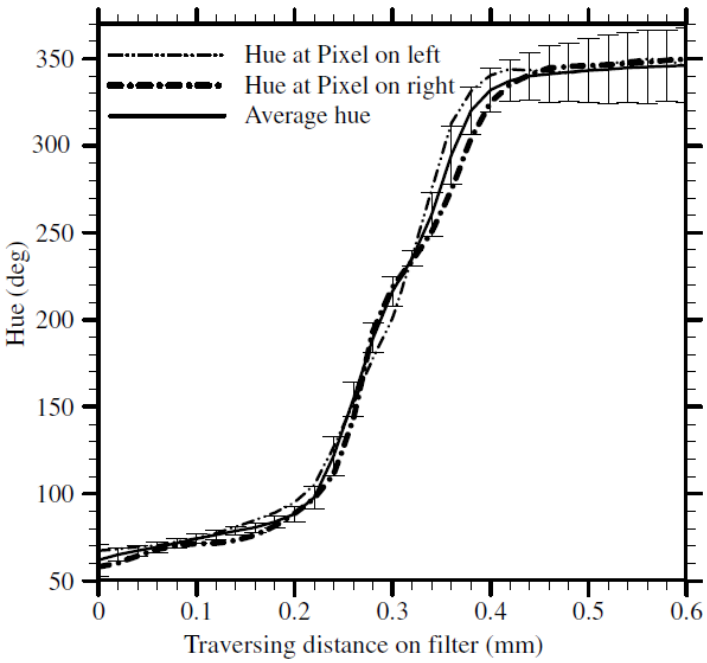

Figure 2.4.1 Filter calibration for hue versus the distance on the filter from previous work [14].

It was important that the background color was precisely located in the center of the filter to ensure there was no bias to one side or the other. The Phantom v611 was used to align the filter and locate the red strip in the center of the filter. Once that was done the location was taken with a micrometer. Then images were captured at .10 mm intervals of the colored part of the filter, from top to bottom. It was important to take measurements in these intervals to ensure there would be minimal hue measurement uncertainties. These images were plugged into the code along with the locations of each image. Deflection up or down is not distinguished in this method. A high order polynomial was used to add a line through the data points. The graphs for the 2.5 mm filter are shown in Figures 2.4.2-3, the graphs for all of the other filters used can be found in Appendix C. Figure 2.4.3 shows the data from Figure 2.4.2 mirrored about the x-axis. This step was taken to show if filter's continuous color spectrum was printed properly and if the images collected were taken at the appropriate locations. If the filter was printed accurately the mirrored graph's data points will overlap and the polynomial line will go directly through the data points in Figure 2.4.3. The data used for these graphs was taken from the center of the images captured. Error bars were incorporated to show the possible deviations.

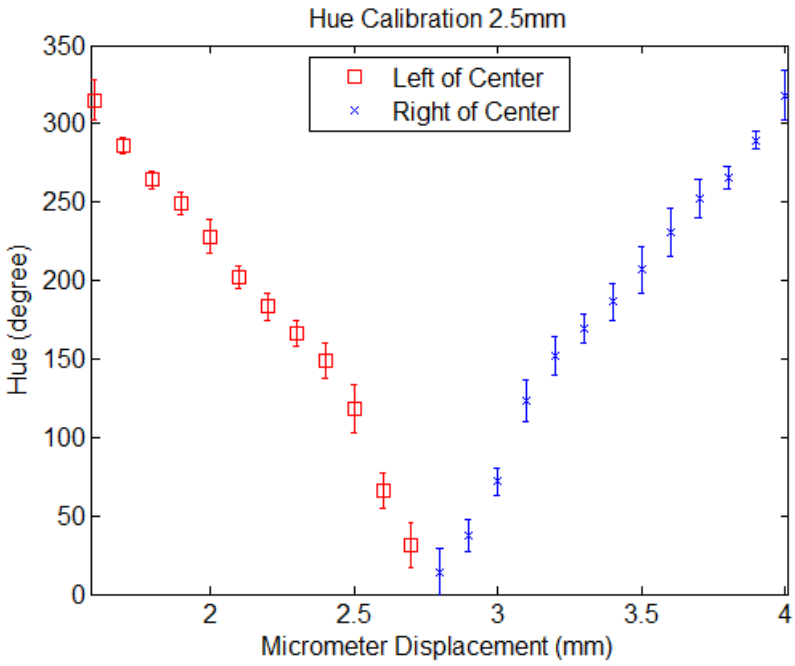

Figure 2.4.2 Hue calibration graph for 2.5 mm symmetric filter.

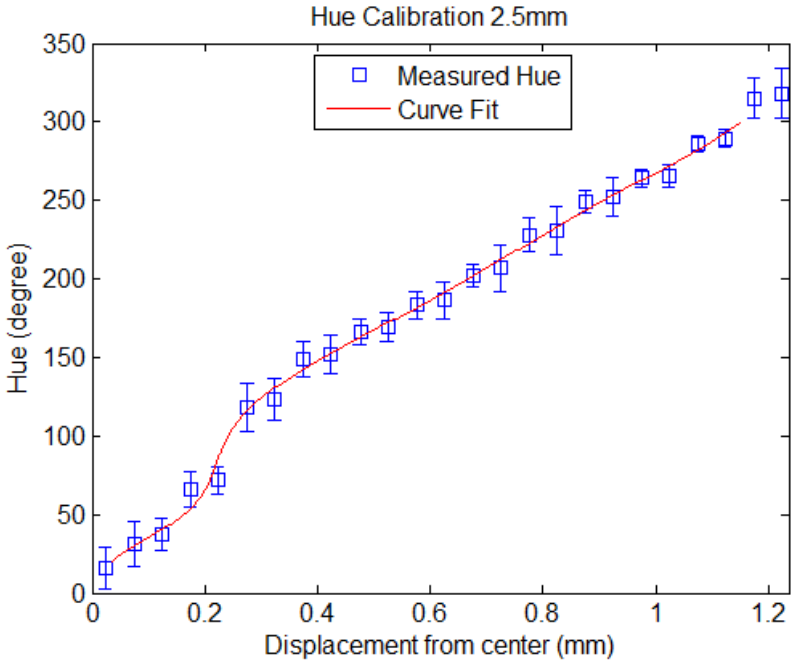

Figure 2.4.3 Mirrored hue calibration graph for 2.5 mm symmetric filter.

As previously mentioned seven different symmetric filter sizes were used to capture a video of 50 injections with a 10 second period. The PCC 2.6 program captured these videos, Figure 2.4.4 is a still frame from one of the videos.

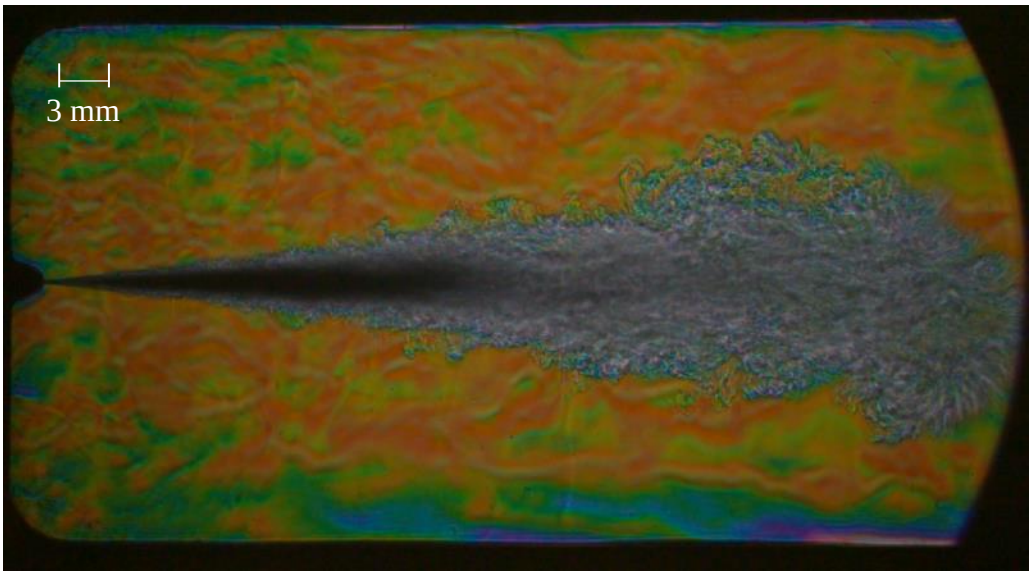

Figure 2.4.4 Snapshot of a single injection using the 1.25mm filter at frame 16 using small aperture.

The second code was designed to average 50 injections over a period of 10 seconds, the resulting injection spray would be more uniform and allow for a clearer depiction of the varying colors throughout the spray. The code also incorporated the conversion from red, green and blue (RGB) to hue, saturation and brightness (HSB). The saturation and brightness levels were set to their max values to allow only the hue color to show since hue is the parameter used to quantify deflection angle. The pixels that were too dark or too saturated were not included. The thresholds were adjusted for each condition but where nominally 15% minimum brightness and 20% minimum saturation. This results in the black regions in the center of the spray where the high liquid density absorbs most of the light and no pixels are included in the average. This step allows for a closer insight as to what the density profile looks like in the center of the spray

where in the above image it is too dark to decipher. Images for the average code for all three filters are shown in Figures 2.4.5-7 below.

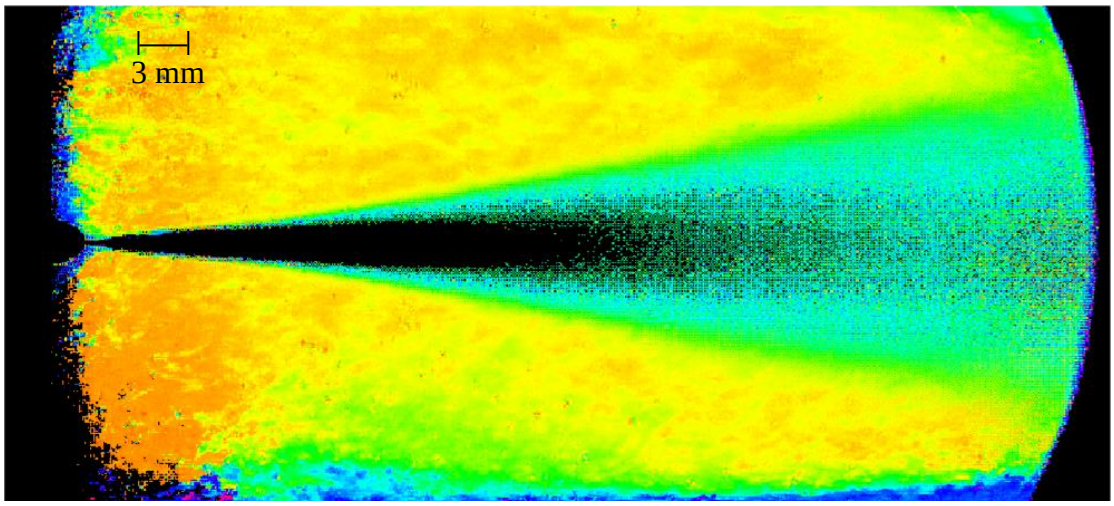

Figure 2.4.5 Snapshot at frame 16 of the average code for 50 injections using the 0.75 mm filter.

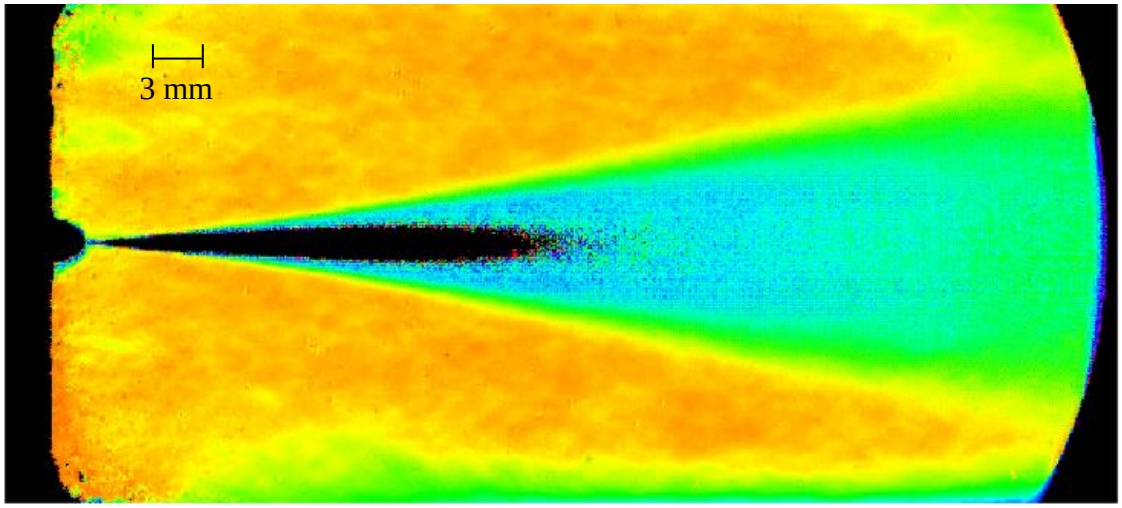

Figure 2.4.6 Snapshot at frame 16 of the average code for 50 injections using the 1.25 mm filter.

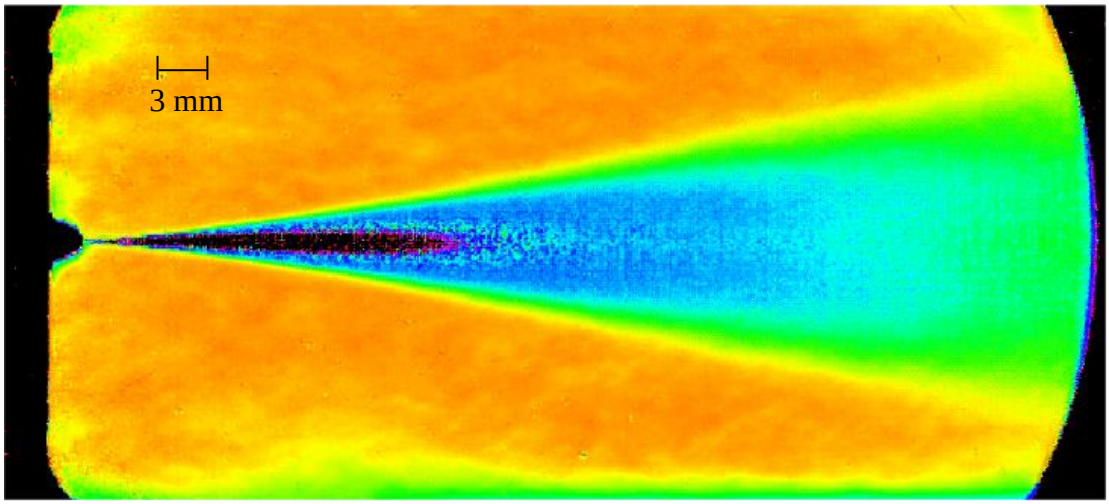

Figure 2.4.7 Snapshot at frame 16 of the average code for 50 injections using the 1.75 mm filter.

As the filters get larger in size the pixels in the center of the spray become more evident. Note the color change from dark blue to purple then black in the center of the spray. The black region, in the center of the fuel spray, is the liquid phase. The density is so high the light cannot penetrate that's why it shows up black. The advantage of using the average code is being able to see over a range of injections the overall density relationship as the spray moves downstream. As opposed to the individual injections, Figure 2.4.4, where the turbulent movement makes it hard to decipher how the fuel is reacting under varying temperatures and filter sizes. Another advantage of using the average image is that it blends in the background colors. Which enables us to see the smaller density gradients along the outside edges of the spray and how they are changing as the fuel moves downstream. Even with the averaging code, the dark regions near the injector with the small aperture prompted the additional work with a larger aperture.

In the case of the 0.75 mm filter, the large black regions downstream of the black core are a result of the saturation threshold rather than the brightness. Near the injector the high density is absorbing light to the point of being dark, but in the 0.75 mm filter the still high density gradients

in the center of the spray downstream seem to be resulting in deflection around the edges of the filter (i.e too large for the filter to detect).

A gray scale code was incorporated to show the liquid boundary using a Mie-scatter image. When paired with the track code (third code) it overlays the Mie-scatter liquid boundary with the videos taken by the Phantom v611. Figure 2.4.8 shows the Mie-scatter image of the liquid length that was overlaid with on a single injection frame with difference described more below. The fourth code, track code, was designed to show the location that was chosen, in terms of xy-coordinates, the hue versus vertical distance and deflection versus vertical distance. The locations used are in terms of a xy-coordinate system, or the distance from the injector tip to downstream of the spray. This was done by finding the xy-coordinate at the injector tip and setting that value to zero. Using the size of the injector tip (known to be 3mm) the pixel per millimeter spatial calibration factor could be determined. Translated to millimeters the locations were 15 mm, 23 mm, 32 mm, 40 mm, 49 mm, 57 mm, 66 mm and 74 mm. The line going through the image shows the 57 mm location, or 57 mm from the injector tip that data was being collected at.

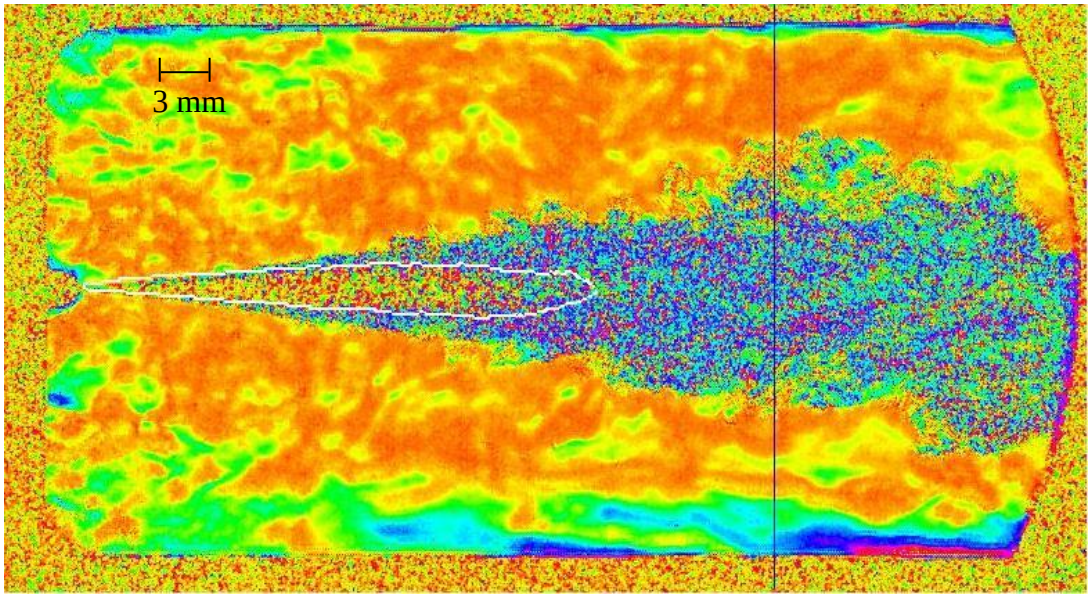

Figure 2.4.8 Mie-scatter liquid boundary overlaid with the footage taken from the Phantom v611.

There is a drastic change in appearance compared to the figures shown for the average code. When the average code is applied all of the injections pixels are averaged together. The result is a smoothed background and smoother transition from the varying colors from the outside of the fuel spray to the center. In Figure 2.4.7 it is difficult to tell how the fuel is mixing as it moves downstream. The air movement creates vortices around the outside edges of the spray and the varying colors of the pixels make it difficult to understand the mixing properties of the fuel spray. For this reason the average code was used. It allows the viewer to see the transition from the liquid phase of the spray to the vapor phase clearly. Also allowing for studies to take place comparing different filter sizes, light penetration and temperature effect.

To further explain the average technique used, Figures 2.4.9 shows snapshots of frames 4, 6, 8, 10, 12, 14, 16, 18, 20 and 22 for one individual spray next to snapshots for the average video. This was done using a 2.5mm symmetrical filter with the large aperture.

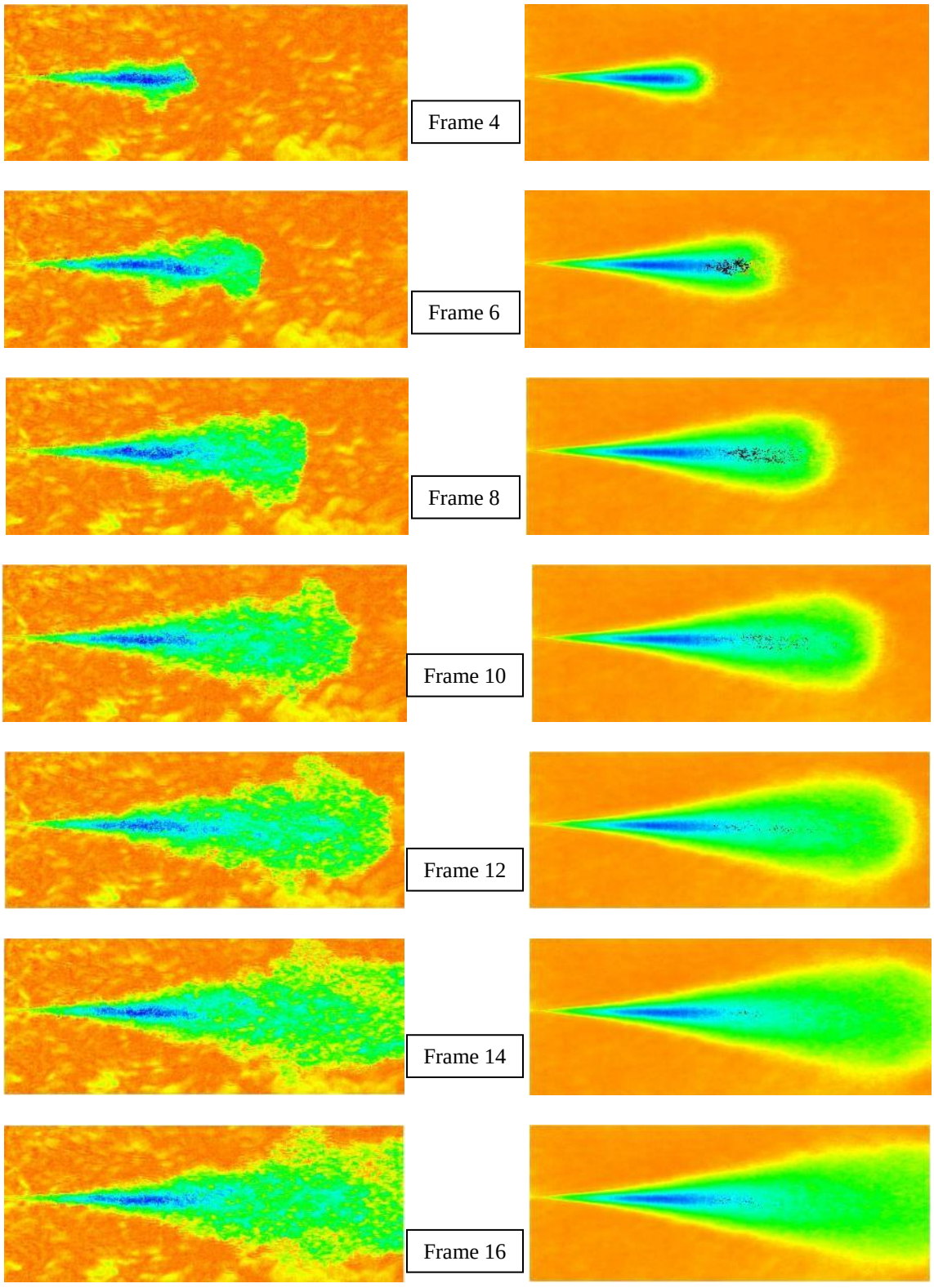
Frame 4
Frame 6
Frame 8
Frame 10
Frame 12
Frame 14
Frame 16

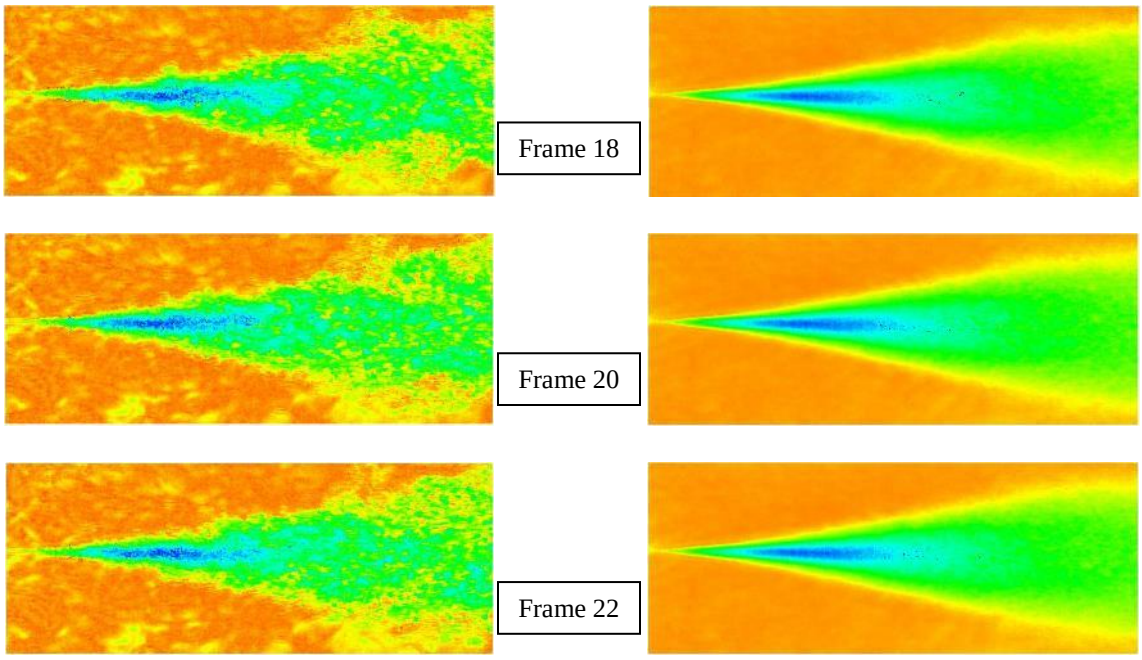

Figure 2.4.9 Comparison of frames from a single injection with frames from the 50 injections averaged together using the 2.5mm symmetrical filter.

The left hand images highlight the vortices pockets as well as the small density gradients along the outside of the spray that are being picked up by the filter. The images on the right blur out some of the vortices so you can see the gradient distribution more clearly as the spray moves down stream. Though the background becomes more uniform one of the disadvantages is the loss of distinction between the small density gradients.

The fourth code was designed to show all of the locations as steps and create a graph to show the relationship between deflection angle and radial position. The graph for the 1.75 mm is shown below in Figure 2.4.10, but will be discussed in the results section.

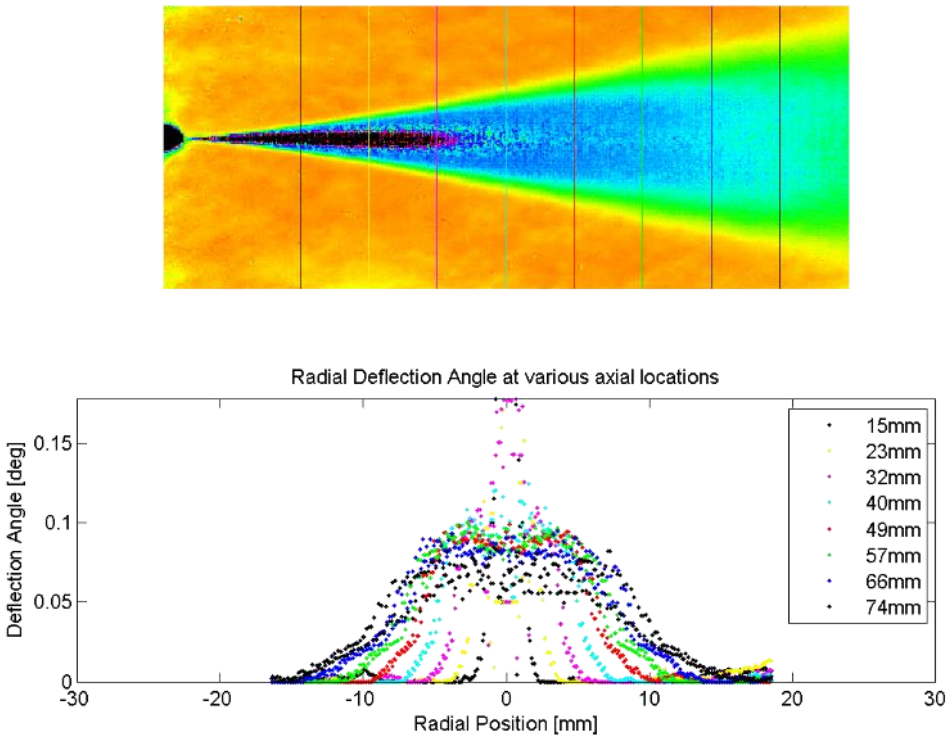

Figure 2.4.10 Radial characterization using a 1.75mm symmetric filter.

Two areas were studied further for the larger aperture using the following filters; 1 mm, 2 mm, 2.5 mm and 5 mm. The filter effect of all four filters at 180°C and the temperature effect for the 2.5 mm filter across temperatures 115°C, 132°C, 160°C and 180°C. The filter effect at 180°C for the 2.5mm filter is shown below in Figure 2.4.11, but will be discussed in the results section.

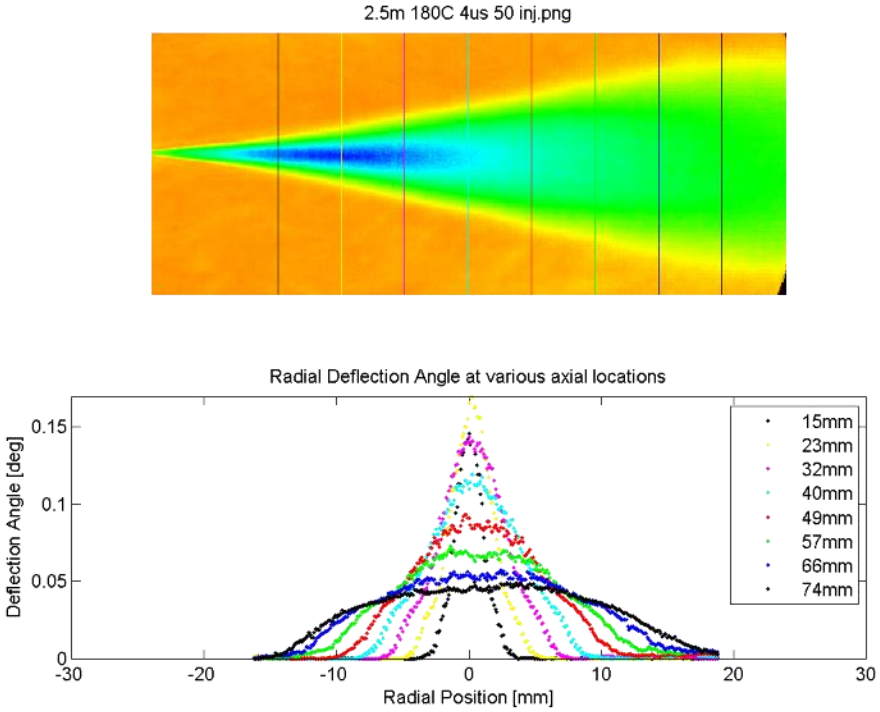

Figure 2.4.11 Radial characterization at 180°C using a 2.5 mm symmetric filter.

3. RESULTS AND DISCUSSION

The experiment was run under various ambient conditions using seven symmetric filters; 0.75 mm, 1.25 mm, 1.00 mm, 1.75 mm, 2 mm, 2.5 mm and 5 mm. Videos were captured for 50 injections over a period 4 minutes with the field of view including the injector tip and as much downstream as possible based on the lenses. Those videos were put through a MATLAB code that averaged all of the sprays on top of one another.

To be able to accurately study the density gradient distribution filter selection is a key component in limiting light diffraction. The filters used with the smaller aperture were 0.75 mm, 1.25 mm and 1.75 mm and were taken with a 90 μs exposure time. The filters used with the larger aperture were 1 mm, 2 mm, 2.5 mm and 5 mm and were taken with a 4 μs exposure time. The locations of all data collected were 15 mm, 23 mm, 32 mm 40 mm, 40 mm, 49 mm, 57 mm, 66 mm and 74 mm downstream of the fuel injector tip.

Figure 3.1 shows a comparison of the filters used with the smaller aperture displaying deflection angle verses radial position. The x axis ranges from -30mm to 30mm, which represents the radial position, the injector tip was located at 0 mm. Essentially, a small filter will better capture the edges of the spray, where the heightened sensitivity is necessary to detect the small outer density gradients. A larger filter will best capture the center of the fuel spray, where the liquid phase is present.

0.75mm_nj.png

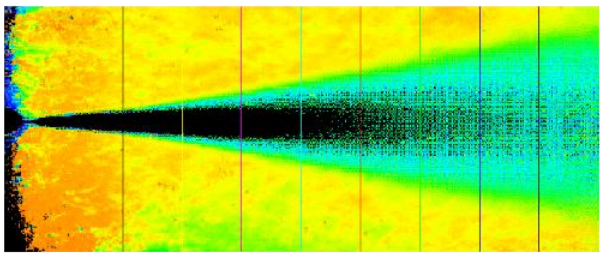

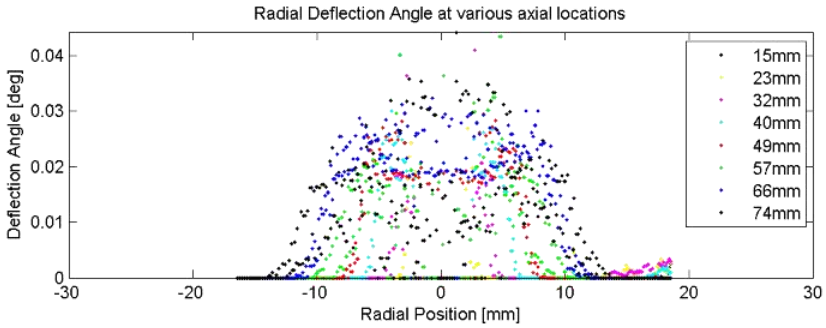

1.25mm_nj.png

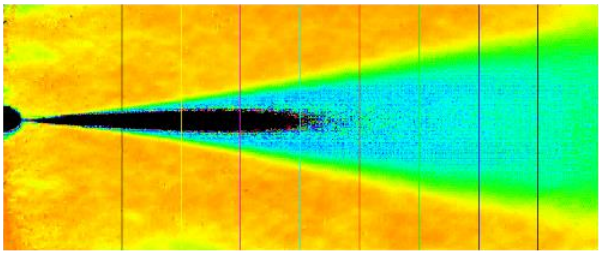

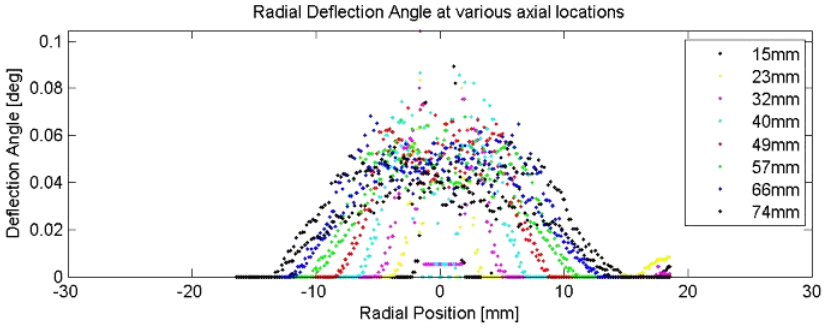

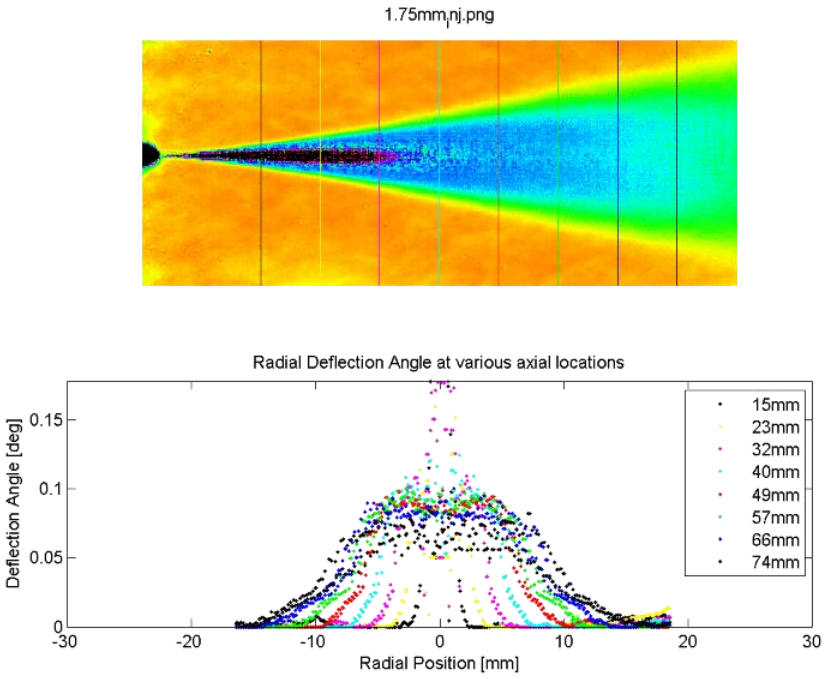

Figure 3.1 Comparison of 0.75mm, 1.25mm and 1.75mm symmetrical filters at 200°C.

As the filter size gets larger the smaller density gradients on the outside edges of the spray begin to blend into the background and the spray appears to be narrower. Due to the reduced light throughput using the smaller aperture all of these figures suffer from poor light penetration in the liquid portion of the spray near the injector. The top image uses a 0.75mm filter; which is too small to show the density gradients in the center of the spray downstream of the liquid region due to light deflecting around it, resulting in a larger black region in the center. However, on the outer edges of the graph a steeper gradient is captured due to the heightened sensitivity capabilities. The middle image uses a 1.25mm filter; the center of the spray is beginning to show the relationship between the liquid phase and the vapor phase of the spray. The 1.75mm filter image shows significant pixel coloration, the larger density gradients are being shown in the magenta and purple. The black region, liquid phase, is becoming more

proportional to the variable profile model. Once again, there is still light limitations due to the aperture size.

Due to the light limitations of the smaller aperture, the larger aperture was used to study the filter effect off all four filters at 180°C and the temperature effect for the 2.5 mm filter across temperatures 115°C, 132°C, 160°C and 180°C.

Figure 3.2 shows the comparison of filter effects at 180°C for all four filters. Taking a look at the graphs, it is clear to see why so much importance is placed on the filter selection. There is a delicate balance between the amount of light deflection and the filter size. The 1 mm filter is too sensitive to capture the density profile in the center of the spray, resulting in a large black region where the liquid phase is present and light deflected around the filter. While the 5 mm filter is not sensitive enough to pick up on the density gradients in center of the spray where the liquid phase is present. The 2 mm and 2.5 mm filters are more ideal for having a balance between capturing the smaller density gradients on the edges of the spray, and the larger density gradients in the center of the spray. There is a stronger correlation to the variable profile model, which tells us that the balance of light penetration to filter size has been reached.

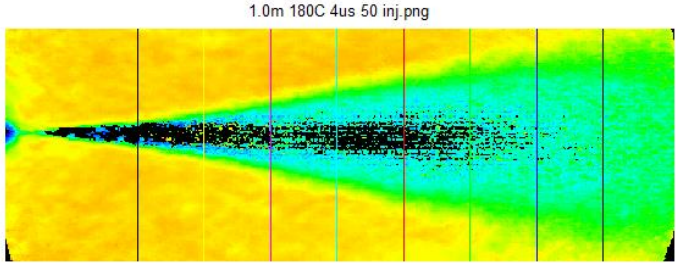
1.0m 180C 4us 50 inj.png

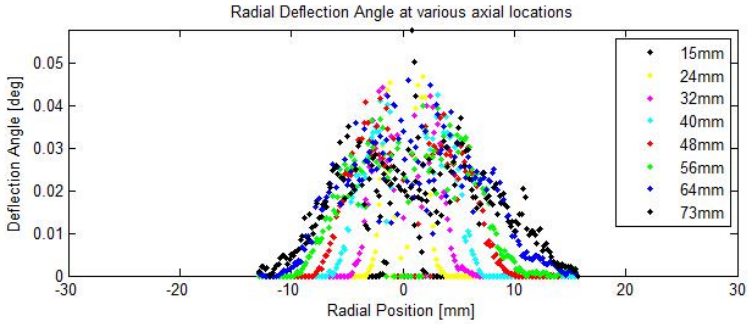
Radial Deflection Angle at various axial locations
Deflection Angle [deg]
Radial Position [mm]
15mm
24mm
32mm
40mm
48mm
56mm
64mm
73mm

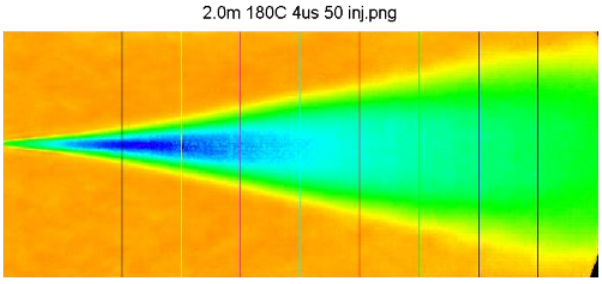
2.0m 180C 4us 50 inj.png

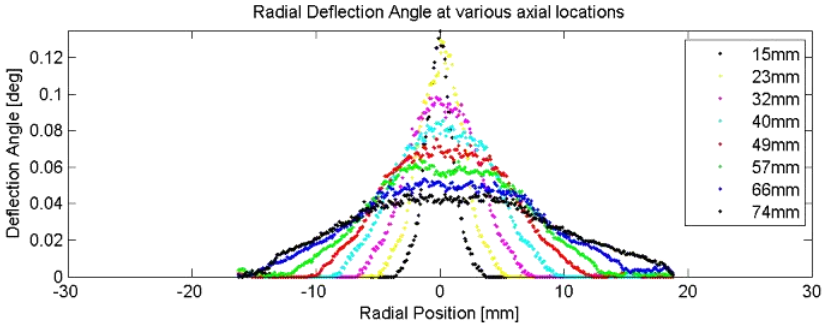
Radial Deflection Angle at various axial locations
Deflection Angle [deg]
Radial Position [mm]
15mm
23mm
32mm
40mm
49mm
57mm
66mm
74mm

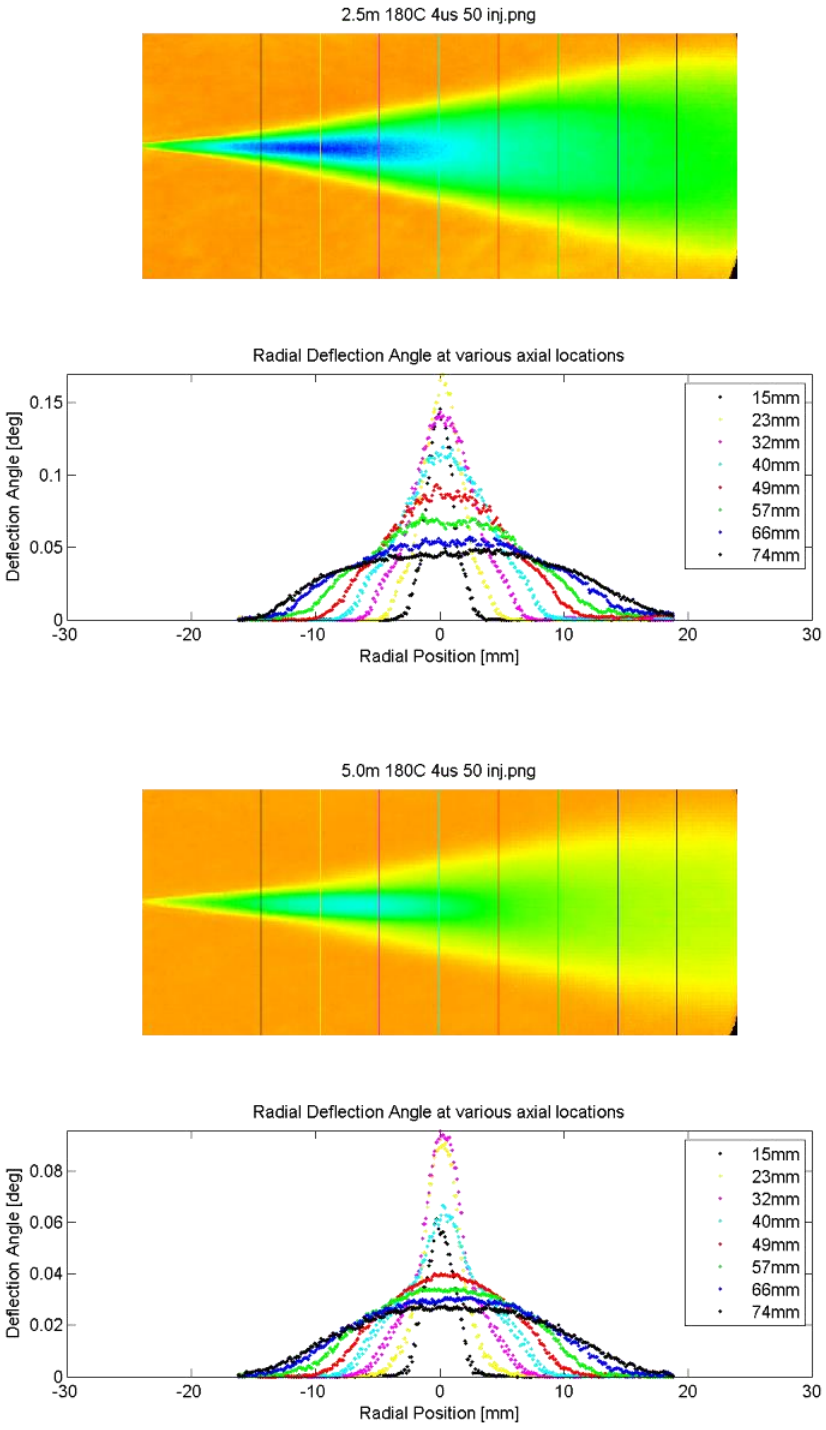

Figure 3.2 Comparison of the radial characterization between the four filters at 180°C.

The 2.5 mm filter was selected to do a temperature sweep to show how temperature effects the radial deflection angle in terms of the radial position. The temperature range was

115℃, 132℃, 160℃ and 180℃. Figure 3.3 shows the resulting graphs. As the temperature increases there is a direct correlation to the liquid phase of the spray. The lighter colors indicate lower overall density (i.e. well mixed/vaporized), as the temperature gets closer to 180℃ it is evident that more sufficient mixing is occurring.

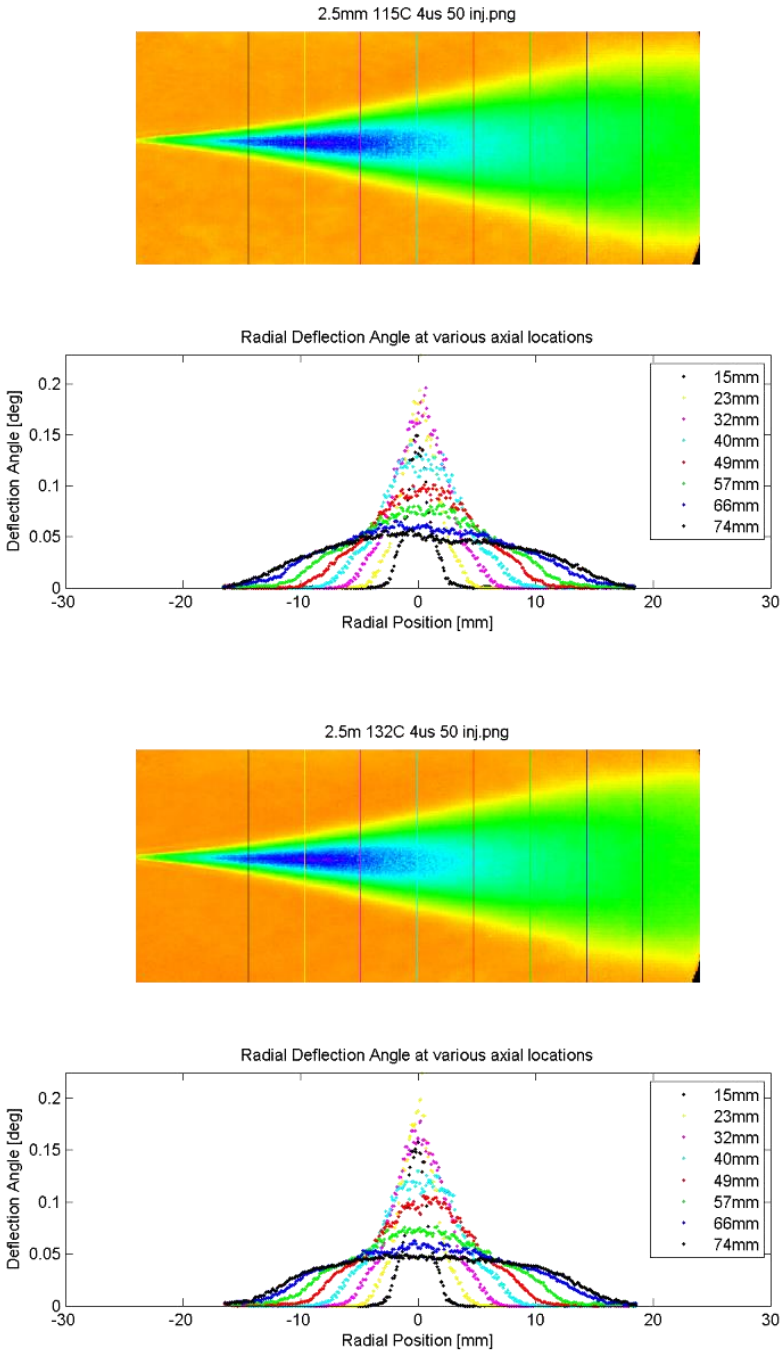

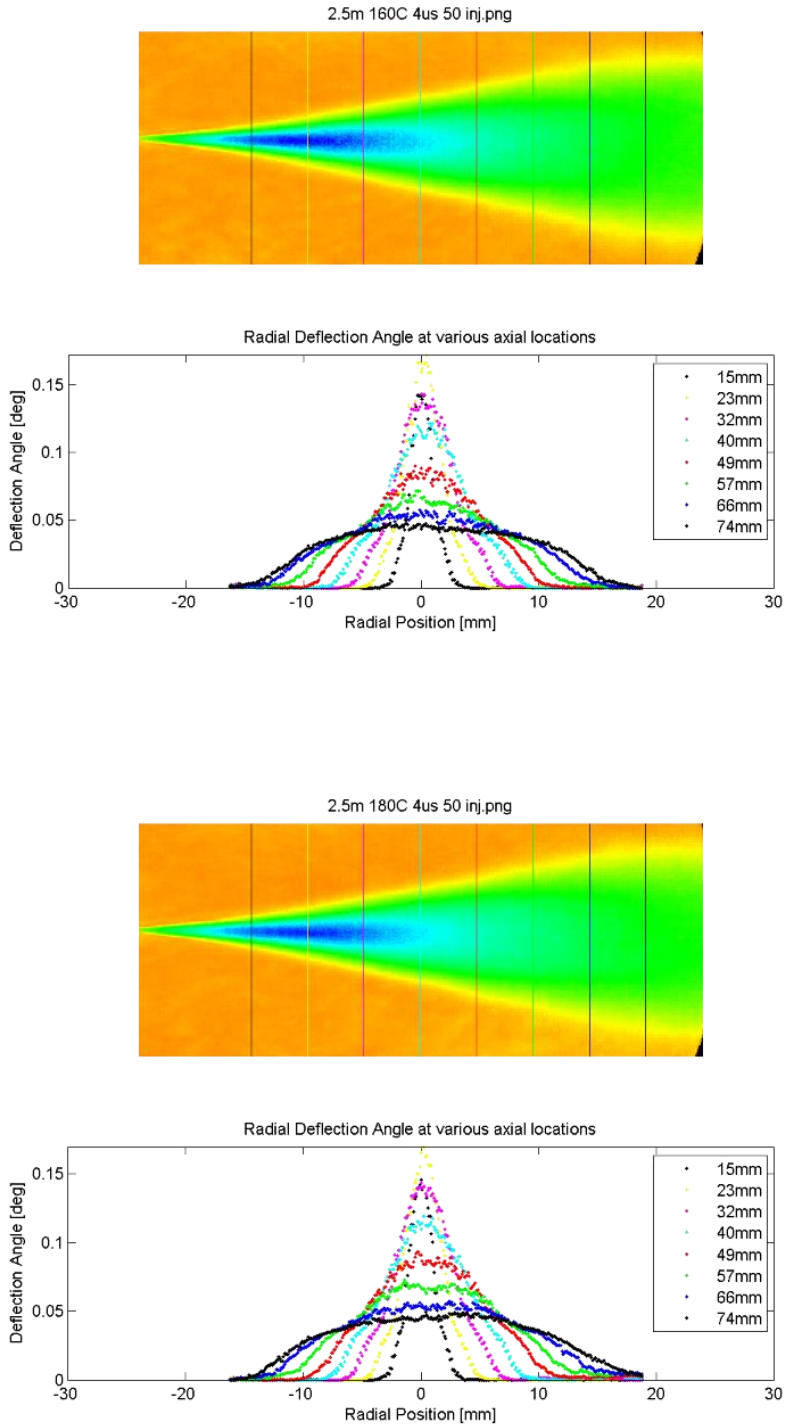

Figure 3.3 Comparison of the radial characterization of varying temperatures using the 2.5mm symmetric filter.

These graphs align with the model proposed by Musculus and Kattke referenced in Figure 1.2.2, shown again below. If sufficient mixing is occurring the density gradient distribution will begin in a thin peak and level out to more of a bell curve as the fuel injection moves downstream. The importance of this knowledge will allow for researchers to understand how the fuel reacts under varying temperatures as it moves downstream. Knowledge gained in this thesis will also aid researchers in finding the balance between light penetration and filter selection to acquire quantitative data.

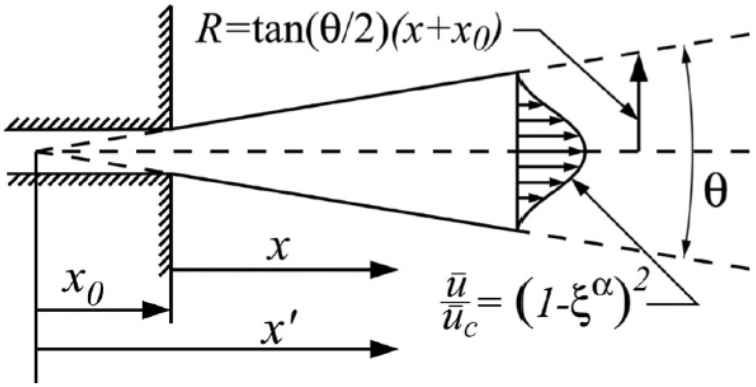

Figure 1.2.2 Musculus and Kattke's variable profile model [8].

4. SUMMARY, CONCLUSIONS AND FUTURE WORK

This thesis describes the rainbow schlieren technique setup and the filter selection process used to acquire quantitative data. There were a few challenges that needed to be overcome to capture data that would help further the characterization of fuel sprays. The alignment of the setup from the light, aperture, lenses, colored filter and the camera took some time to perfect. Many images were taken over a year long period before we determined the setup was aligned correctly. Filter selection was another area that took time to research thoroughly. Filter sizes ranged from 0.50 mm to 5 mm for both symmetrical and non-symmetrical makeup. Filter calibrations and images were collected for most of the filters we had access too, under varying temperatures and pressures, before we could determine which ones to use and then which aperture to pair with which filter. The coding made it possible to further understand the limitations as well as advantages to using different filter sizes with the two different aperture sizes. The conclusion of this thesis determined that the 2.5 mm symmetric filter paired with the larger, 100 μm by 3 mm, aperture provided important information that will aid future research.

Understanding the density gradient profile will aid research in terms of fuel characterization. The more that is understood about this profile the more researchers can apply this knowledge to enhance sufficient mixing in diesel engines. As previously stated, unlike gasoline engines, diesel engines time frame to mix air and fuel is limited. It is imperative to understand at what moment and what temperature the most sufficient mixing will occur. This will lead to better fuel efficiency in terms of increase in power as well as lowing toxic emissions.

This thesis focused on low temperature combustion, future work will look into conditions similar to peak cylinder compression conditions including reacting sprays. The combined knowledge will give an expanded view on the density gradient profile.

REFERENCES

[1] G. Templeton (2013) Low temperature combustion could drive efficient, clean diesel engines back into the limelight.

[2] D.L. Siebers, (1999) Scaling Liquid-Phase Fuel Penetration in Diesel Sprays Based on Mixing-Limited Vaporization, (SAE Paper No. 1999-01-0528).

[3] J.E. Dec, (1997) A conceptual model of DI diesel combustion based on laser-sheet imaging, SAE Transactions - Journal of Engines. 106 (SAE Paper No. 970873) 1319-1348.

[4] A. Adam, P. Leick, G. Bittlinger, C. Schulz, (2008) Visualization of the evaporation of a Diesel spray using combined Mie and Rayleigh scattering techniques, 14th International Symposium on Applications of Laser Techniques to Fluid Mechanics (Itces No. 2007-01-0647).

[5] K.C. James, J. Wang, M.C. Maynard, Z.B. Morris, B.T. Fisher, (2014) Development of a High-Pressure, High-Temperature, Optically Accessible Continuous-Flow Vessel for Fuel-Injection Experiments, Journal of Engineering for Gas Turbines and Power. 136 (9) 091512-091512.

[6] L.M. Pickett, S. Kook, T.C. Williams, (2009) Transient Liquid Penetration of Early-Injection Diesel Sprays, SAE Int.J.Engines. 2 785-804.

[7] L.M. Pickett, J. Manin, C.L. Genzale, D.L. Siebers, M.P.B. Musculus, C.A. Idicheria, (2011) Relationship Between Diesel Fuel Spray Vapor Penetration/Dispersion and Local Fuel Mixture Fraction, SAE Int. J. Engines. 4 (SAE Paper No. 2011-01-0686) 764-799.

[8] M.P.B. Musculus, K. Kattke, (2009) Entrainment Waves in Diesel Jets, SAE Int. J. Engines. 2 (SAE Paper No. 2009-01-1355) 1170-1193.

[9] C.A. Idicheria, L.M. Pickett, (2007) Quantitative Mixing Measurements in a Vaporizing Diesel Spray by Rayleigh Imaging, (SAE Paper No. 2007-01-0647).

[10] L.M. Pickett, J. Manin, C.L. Genzale, D.L. Siebers, M.P.B. Musculus, C.A. Idicheria, (2011) Relationship Between Diesel Fuel Spray Vapor Penetration/Dispersion and Local Fuel Mixture Fraction, SAE Int. J. Engines. 4 (SAE Paper No. 2011-01-0686) 764-799.

[11] Gurpreet Singh, Overview of the DOE Advanced Combustion Engine, R&D (2011 Merit Review).

[12] T. Johnson, Diesel engine emissions and their control, (2008 Johnson Matthey Technology Review).

[13] P.K. Panigrahi, K. Muralidhar, (2012) Schlieren and shadowgraph methods in heat and mass transfer, Springer Publication (2012).

[14] P.S. Solhe, A.K. Agrawal, 2009b, "Density measurements in a supersonic microjet using miniature rainbow schlieren deflectometry," AIAA Journal, 47(4), 830-838.

[15] K. Muralidhar, P.K. Kanpur, "Color schlieren technique." National Program for Technology Enhanced Learning. 07 May 2012. Lecture.

[16] A.K. Agrawal, N.K. Butuk, S.R. Gollahalli, D. Griffin, (1998) Three-dimensional rainbow schlieren tomography of a temperature field in gas flows, Appl. Opt. 37 (3) 479-485.

[17] A.K. Agrawal, K. Alammar, S. Gollahalli, (2002) Application of rainbow schlieren deflectometry to measure temperature and oxygen concentration in a laminar gas-jet diffusion flame, Exp. Fluids. 32 (6) 689-691.

[18] K. Al-Ammar, A.K. Agrawal, S.R. Gollahalli, D. Griffin, (1998) Application of rainbow schlieren deflectometry for concentration measurements in an axisymmetric helium jet, Exp. Fluids. 25 (2) 89-95.

[19] A.K. Agrawal, B.W. Albers, D.W. Griffin, (1999) Abel inversion of deflectometric measurements in dynamic flows, Appl. Opt. 38 (15) 3394-3398.

[20] P.S. Greenberg, R.B. Klimek, D.R. Buchele, (1995) Quantitative rainbow schlieren deflectometry, OSA 34 (19) 3810-3825.

[21] J. Wang, Experimental measurements of n-heptane liquid length and spray cone angle for early direct injection low temperature conditions relevant to diesel engines in an optically accessible constant pressure flow vessel. Master Thesis, University of Alabama, Tuscaloosa Alabama.

APPENDIX A. MATLAB CODES

Hue Calibration Code:

```
clc
clear all
Files = ls('*.bmp');

calibrationrows=4;
calibrationcols=50;

for i=1:numel(Files(:,1))

        loc(i)=str2double(Files(i,1:strfind(Files(i,:), 'mm')-1));
        image = rgb2hsv(imread(Files(i,:)));
        width = size(image,2);
        height = size(image,1);
        for row=1:calibrationrows
            for col=1:calibrationcols
                hue(col,row,i) = image(height/2-
calibrationcols/2+col,width/2-calibrationrows/2+row,1)*360;
                location(col,row,i)=loc(i);
            end
        end

        hueavg(i)=mean(hue(location==loc(i)));
end

mid=(max(loc)+min(loc))/2-.05;
tophueavg=hueavg(loc>mid);
toploc=loc(loc>mid);
bothueavg=hueavg(loc<=mid);
botloc=loc(loc<=mid);

m=(botloc(end)-botloc(end-1))/(bothueavg(end)-bothueavg(end-1));
boteqlloc=m*(tophueavg(1)-bothueavg(end))+botloc(end);
middleoffilter=(toploc(1)+boteqlloc)/2;

figure(3)
plot(tophueavg,toploc,'rx',bothueavg,botloc,'bs')

locfinal = [abs(loc-middleoffilter)];
finaldata= sort([hueavg' locfinal'],2,'ascend');
hueavg = finaldata(:,2);
locfinal = finaldata(:,1);

xlabel('Hue (degree)');
ylabel('Displacement (mm)');
```

```
title('Hue Calibration');

figure(2)
huetodistancebestfit = polyfit(hueavg,locfinal,8);
f = polyval(huetodistancebestfit,hueavg);

huetest=[20:1:350];
xtest=polyval(huetodistancebestfit,huetest);

plot(hueavg,locfinal,'bs',hueavg,f,'rx',huetest,xtest)

xlabel('Hue (degree)');
ylabel('Displacement (mm)');
title('Hue Calibration');

folderloc = strfind(pwd, '\');
folder = pwd;
outfile = strcat(folder(folderloc(end)+1:end),'.mat');
save(outfile,'huetodistancebestfit','-mat')
```

Average Code:

```
LoadPhantomLibraries();
RegisterPhantom(true); %Register the Phantom dll's ignoring connected
cameras.
%                       %Use this function once at the begining of your work
clear all



%
load('\\uafs1.ua-net.ua.edu\share\COE\BittleLabShare\Spray Chamber
Data\Filter Calibration Images\filtercalibrations.mat',...
    'calibration200mmsym','calibration125mmsym',...
    'calibration100mmsym');

filelist=ls('2.5*.cine')
[count,~]=size(filelist);

for(i=1:count)
    colorfilename=filelist(i,:);



filtersize=[colorfilename(1) colorfilename(3)];
calfile=whos(['*' filtersize '*']);
calibration=eval(calfile.name);

if(isempty(strfind(colorfilename,'downstream')))
%for steady ensamble average use start 20 end 35
startframe =20; %range for near injector
endframe= 20;
else
startframe =40; %range for downstream
endframe= 50;
end


pccstartframe = 1; %was set to 1
nInjections=50; %was set to 50
nFramesperinjection=40;

croptop=60;
cropbot=20;
cropright=55;
cropleft=45;
%2.0 sat=.25 val= .15
%1.25 sat .3 val .25
%1.0 sat .5 val .3
%0.75 sat .5 val .4

satthreshold =.25; %.25 seems good for high temp, 35 for low
valthreshold=.15; %.15

nFrames = nInjections*nFramesperinjection;
```

```
previmage=ReadCineFileImage(colorfilename, 1+startframe-1+pccstartframe,
false);
[vidHeight,vidWidth,~]=size(previmage);

vidHeight=vidHeight-croptop-cropbot;
vidWidth=vidWidth-cropleft-cropright;
%save one raw injection
movraw(1:nFramesperinjection) = ...
    struct('cdata',zeros(vidHeight,vidWidth, 3,'uint16'));

for(i=startframe:endframe)
[matlabImColor, origIm] = ReadCineFileImage(colorfilename, i+pccstartframe,
false);
movraw(i).cdata = matlabImColor(croptop:vidHeight+croptop-
1,cropleft:cropleft+vidWidth-1,:);
figure(50)
hsvframe=rgb2hsv(movraw(i).cdata);
hue=hsvframe(:,:,1);
sathsv=cat(3,hue,ones(vidHeight,vidWidth),ones(vidHeight,vidWidth));
imshow(hsv2rgb(sathsv))
end

%%% average code
movavg_hsv(1:nFramesperinjection) = ...
    struct('hue',zeros(vidHeight,vidWidth,'double'));

tic
for k = startframe : endframe
   tic
   (k-startframe+1)/(endframe-startframe+1)*100
   pixelcount=zeros(vidHeight,vidWidth,'uint16');
    for i = 1:nInjections
        [matlabImColor, origIm] = ReadCineFileImage(colorfilename, ((i-
1)*nFrames/nInjections+k+pccstartframe-1), false);
        hsvframe=rgb2hsv(matlabImColor(croptop:vidHeight+croptop-
1,cropleft:cropleft+vidWidth-1,:));

        hue=hsvframe(:,:,1);

checkbright=(hsvframe(:,:,2)>satthreshold&hsvframe(:,:,3)>valthreshold);
        pixelcount=pixelcount+cast(checkbright,'uint16');
        movavg_hsv(k).hue = movavg_hsv(k).hue+hue.*checkbright;
    end
    movavg_hsv(k).hue=movavg_hsv(k).hue./cast(pixelcount,'double');
    toc



sathsv=cat(3,movavg_hsv(k).hue,ones(vidHeight,vidWidth),ones(vidHeight,vidWid
th));
    figure(2)

    avgimg=hsv2rgb(sathsv);
```

```
    imshow(avgimg)
    title(['frame# ' sprintf('%d',k)])
    %BittleInversion(movavg_hsv(k).hue,calibration)
   % mov(k-startframe+1)=getframe(gcf);
    pause(0.1)
end

%Only applies to steady portion of spray
movavgtotalframe_hsv = zeros(vidHeight,vidWidth,'double');
pixelcount=zeros(vidHeight,vidWidth,'uint16');
for k = startframe : endframe
frame=movavg_hsv(k).hue;
checknan=isnan(frame);
pixelcount=pixelcount+cast(~checknan,'uint16');
frame(checknan)=0;
movavgtotalframe_hsv = movavgtotalframe_hsv + frame;
end
movavgtotalframe_hsv = movavgtotalframe_hsv./cast(pixelcount,'double');

figure(3)
imshow(hsv2rgb(cat(3,movavgtotalframe_hsv,ones(vidHeight,vidWidth),ones(vidHe
ight,vidWidth))))
title(colorfilename)
toc

print([colorfilename(1:find(colorfilename=='.',1,'last')-1) '.png'],'-dpng')
%movie2avi(mov, '2.00mm 180C Spray Video.avi','compression','none', 'fps',
5);
end
```

Track Code:

```
%read png file of average spray behavior and generate a contour map.
clear all;

injdia_px=30;
injdia_mm=3;
mm_per_px = injdia_mm/injdia_px;

focalLength=250; %mm
injtip=27;
flip=0;

steps=10;

filelist=ls('2.0*contour.png');
[count,~]=size(filelist);
for(i=count:-1:1)
delete(filelist(i,:));
end


%Large Aperture
% load('\\uafs1.ua-net.ua.edu\share\COE\BittleLabShare\Spray Chamber
Data\Filter Calibration Images\filtercalibrations.mat',...
%     'calibration100mmsym','calibration200mmsym',...
%     'calibration250mmsym','calibration500mmsym');

%Small Aperture
load('\\uafs1.ua-net.ua.edu\share\COE\BittleLabShare\Spray Chamber
Data\Filter Calibration Images\filtercalibrations.mat',...
    'calibration075mmsym','calibration125mmsym',...
    'calibration200mmsym');


filelist=ls('2.0*.png');
[count,~]=size(filelist);

%code to run inj and downstream by sorting file list... need inj to go
%first for background color calculation and center

for(i=count:-1:1)
    filename=filelist(i,:);

list = who('cal*');
filtersize=[filename(1) filename(3)];
calfile=whos(['*' filtersize '*']);
calibration=eval(calfile.name);

avgimg = imread(filename);
[height,width,~]=size(avgimg);
```

```
trimtop=225;
trimbottom=320;
trimleft=200;
trimright=150;
avgimg=avgimg(trimtop:height-trimbottom,trimleft:width-trimright,:);
 [height,width,~]=size(avgimg);

if(flip)
    tempavgimg=avgimg;
    for(j=1:width)
    avgimg(:,j,:)=tempavgimg(:,end-j+1,:);
    end
end


if(i==count)
backgroundsnip=rgb2hsv(avgimg);
huebackground=mean(mean(backgroundsnip(28:92,189:315,1)))*360; %good for left
to right spray

xbackground = polyval(calibration,huebackground);
end

figure(i)
clf

subplot(2,1,1)
imshow(avgimg)
hold on;
title(filename)


hsv_avgimg = rgb2hsv(avgimg);
hue=hsv_avgimg(:,:,1)*360;

[height,width,~]=size(hue);
plotsteps=floor(width/steps);
plotstart=2*plotsteps;
%DeflectionData=zeros(height+3,steps,count);
rad=(1:height);
linecolor=['k.','y.','m.','c.','r.','g.','b.','k.'];
colorcount=1;
for(Dist=plotstart:plotsteps:(steps-1)*plotsteps)
    loc = (Dist-injtip)*mm_per_px;
    subplot(2,1,1)
    hold on;
    plot([Dist Dist],[1 height],linecolor(2*colorcount-1))
    subplot(2,1,2)

    x = max(polyval(calibration,hue(:,Dist))-xbackground,0);
    angle=x/focalLength*180/pi;
    edges=find(angle>0.01);
    if(~isempty(edges))
    if(edges(1)~=1)
    coneangle=atand((edges(end)-edges(1))/2/(Dist-injtip))*2;
```

```
        if(colorcount==1&&i==count)
            center=(edges(end)+edges(1))/2;
        end
    end
    else
        coneangle=nan;
    end

    plot((rad-center)*mm_per_px,angle,linecolor(2*colorcount-1:2*colorcount))
    hold on;
    ylabel('Deflection Angle [deg]')
    xlabel('Radial Position [mm]')

    title('Radial Deflection Angle at various axial locations')
    legendtext{colorcount}=sprintf('%.0fmm',ceil(loc));

    DeflectionData(1,1,i)=str2double(filtersize);
    DeflectionData(1,1+colorcount,i)=coneangle;
    DeflectionData(2,1+colorcount,i)=ceil(loc);
    DeflectionData(3:numel(angle)+2,1+colorcount,i)=angle;
    DeflectionData(3:numel(angle)+2,1,i)=(rad-center)*mm_per_px;
    colorcount=colorcount+1;

end
xlim([-30 30])
ylim([0 inf])
legend(legendtext)
%ax = gca;
%ax.XTick = [0 50 100 150 200 250 300];
%ax.YTick = [-200 -150 -100 -50 0 50 100 150 200];
hold off;
print([filename(1:find(filename=='.',1,'last')-1) ' contour.png'],'-dpng')
save([filename(1:find(filename=='.',1,'last')-1)
'data.mat'],'DeflectionData')
end
```

APPENDIX B. HUE CALIBRATION GRAPHS

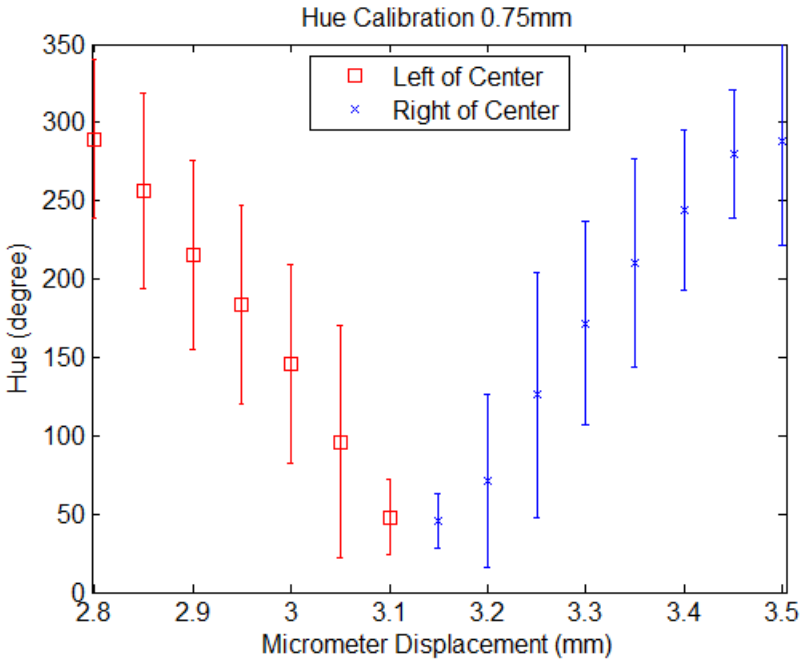

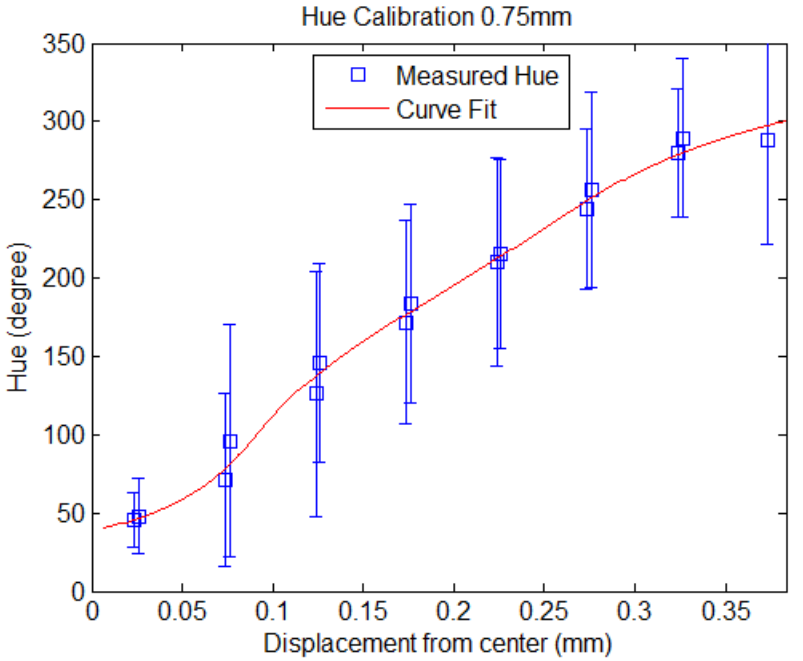

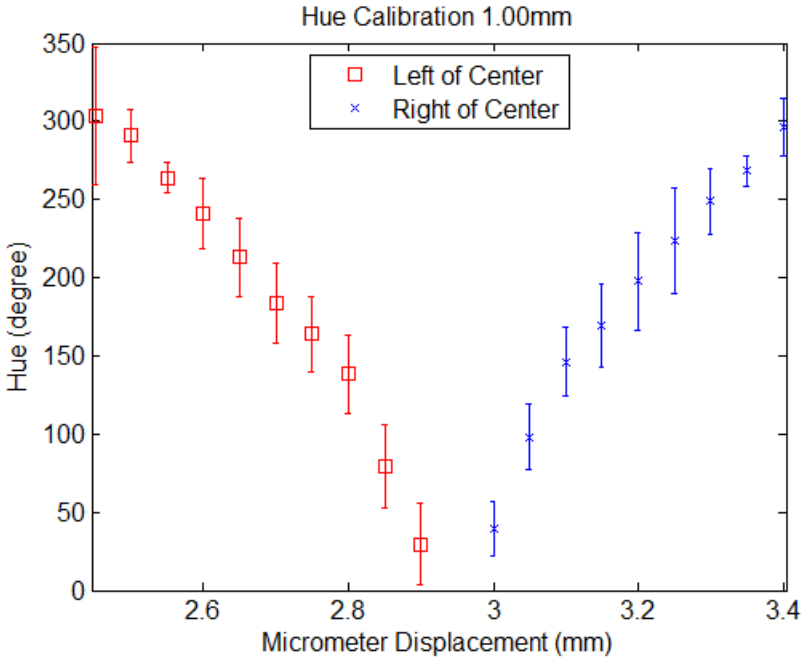
Hue Calibration 1.00mm
Left of Center
Right of Center
Hue (degree)
Micrometer Displacement (mm)
0
50
100
150
200
250
300
350
2.6
2.8
3
3.2
3.4

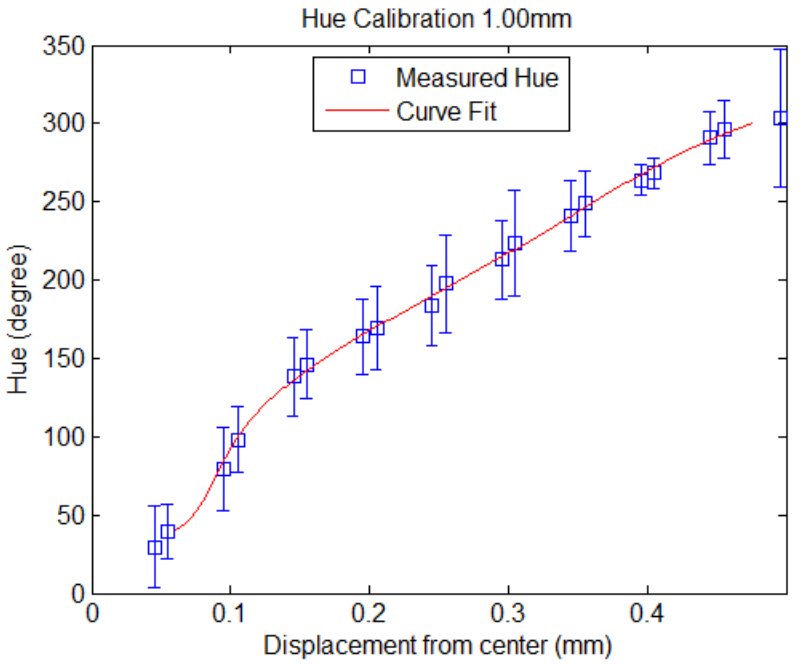
Hue Calibration 1.00mm
Measured Hue
Curve Fit
Hue (degree)
Displacement from center (mm)
0
50
100
150
200
250
300
350
0
0.1
0.2
0.3
0.4

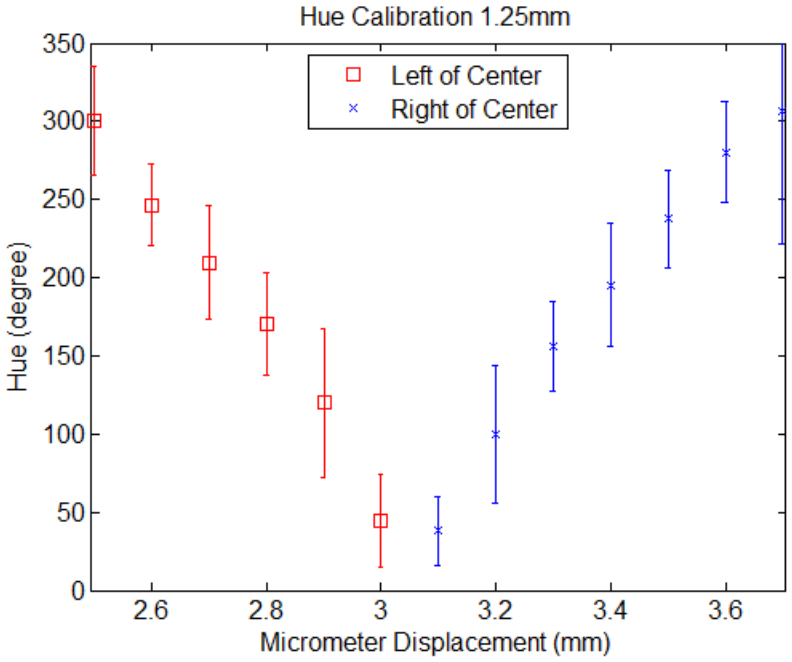
Hue Calibration 1.25mm
Left of Center
Right of Center
Hue (degree)
Micrometer Displacement (mm)
0
50
100
150
200
250
300
350
2.6
2.8
3
3.2
3.4
3.6

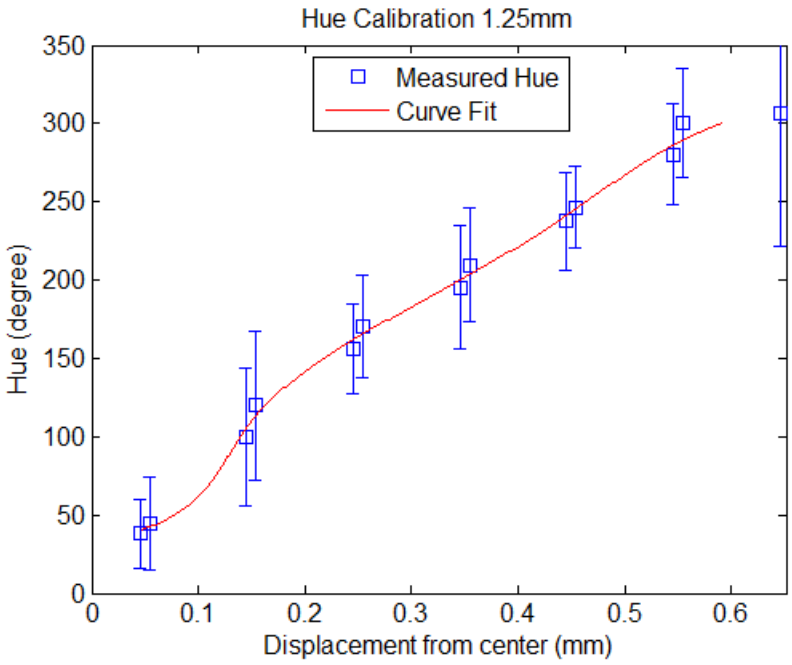
Hue Calibration 1.25mm
Measured Hue
Curve Fit
Hue (degree)
Displacement from center (mm)
0
50
100
150
200
250
300
350
0
0.1
0.2
0.3
0.4
0.5
0.6

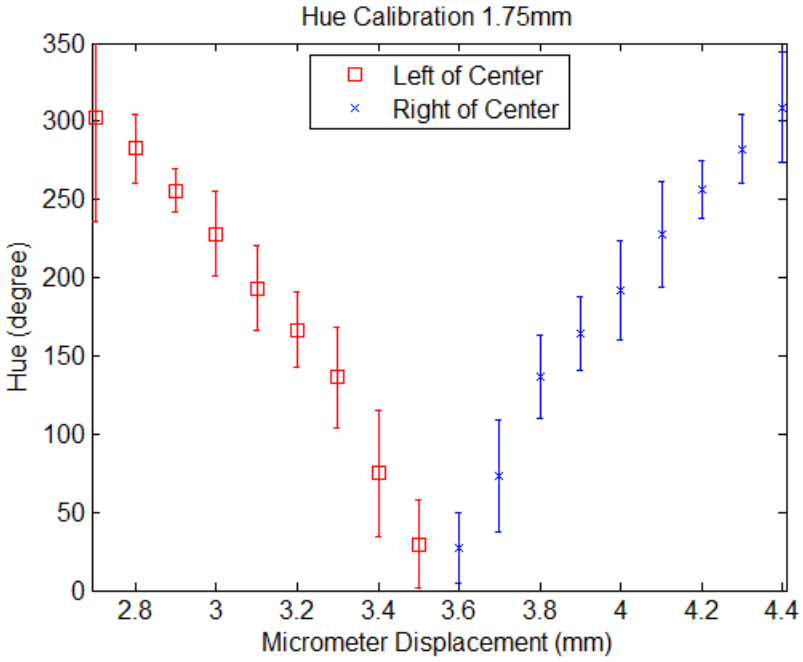
Hue Calibration 1.75mm
Left of Center
Right of Center
Hue (degree)
Micrometer Displacement (mm)
0
50
100
150
200
250
300
350
2.8
3
3.2
3.4
3.6
3.8
4
4.2
4.4

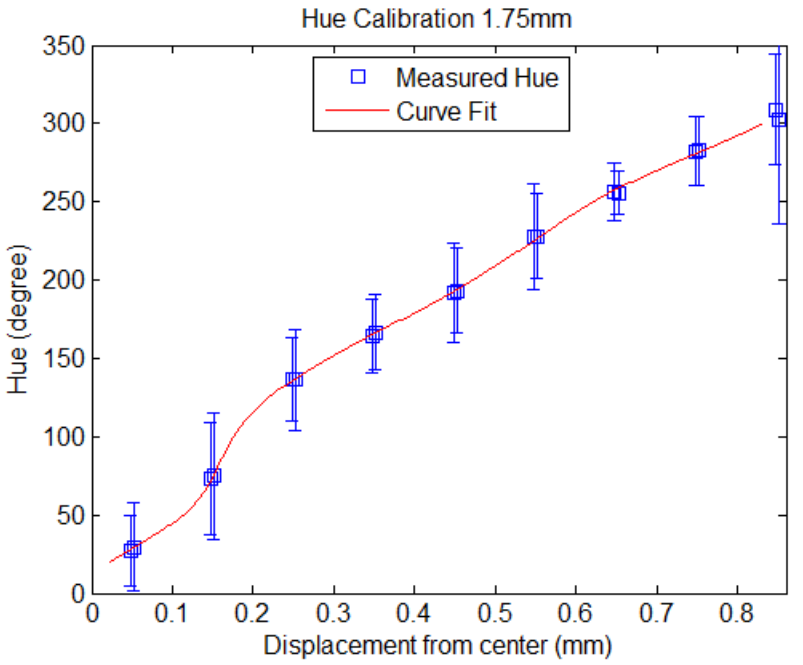
Hue Calibration 1.75mm
Measured Hue
Curve Fit
Hue (degree)
Displacement from center (mm)
0
50
100
150
200
250
300
350
0
0.1
0.2
0.3
0.4
0.5
0.6
0.7
0.8

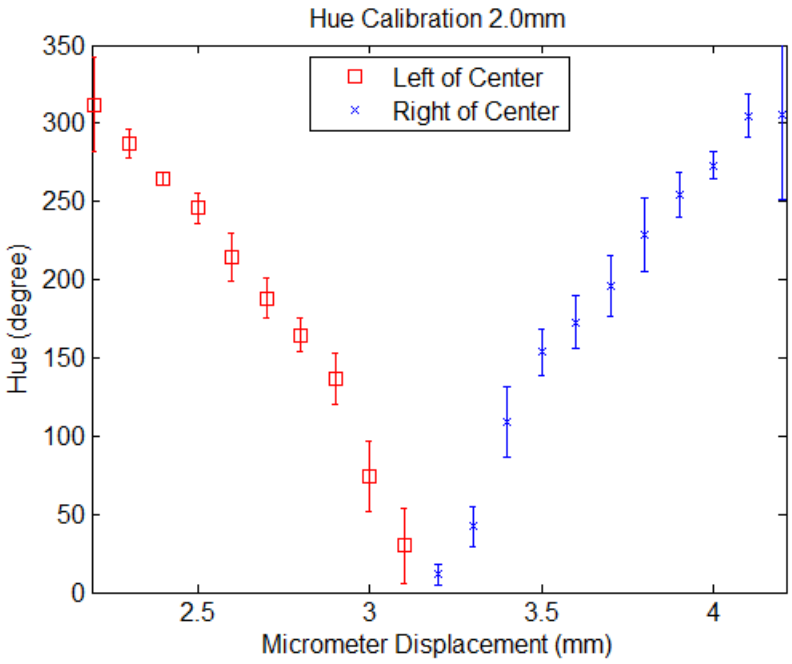
Hue Calibration 2.0mm
Left of Center
Right of Center
Hue (degree)
Micrometer Displacement (mm)
0
50
100
150
200
250
300
350
2.5
3
3.5
4

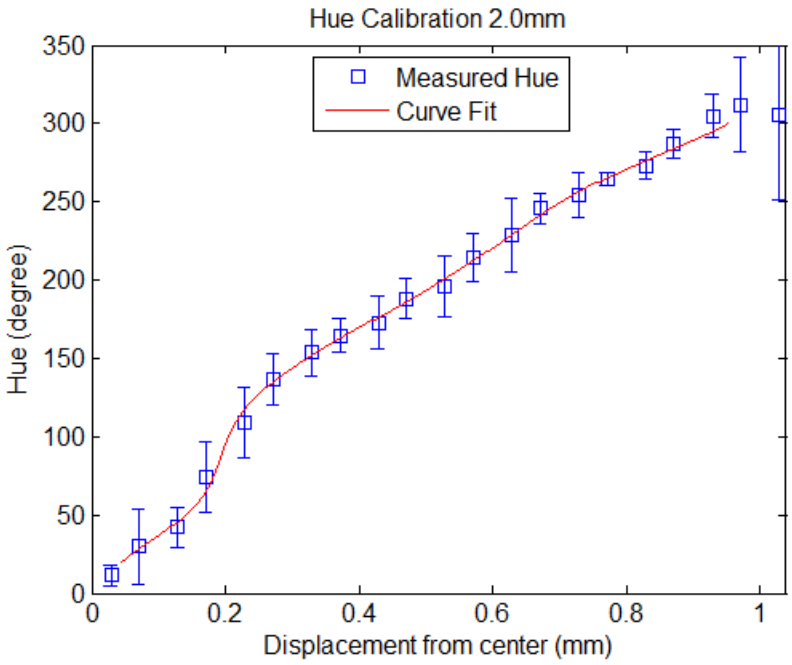
Hue Calibration 2.0mm
Measured Hue
Curve Fit
Hue (degree)
Displacement from center (mm)
0
50
100
150
200
250
300
350
0
0.2
0.4
0.6
0.8
1

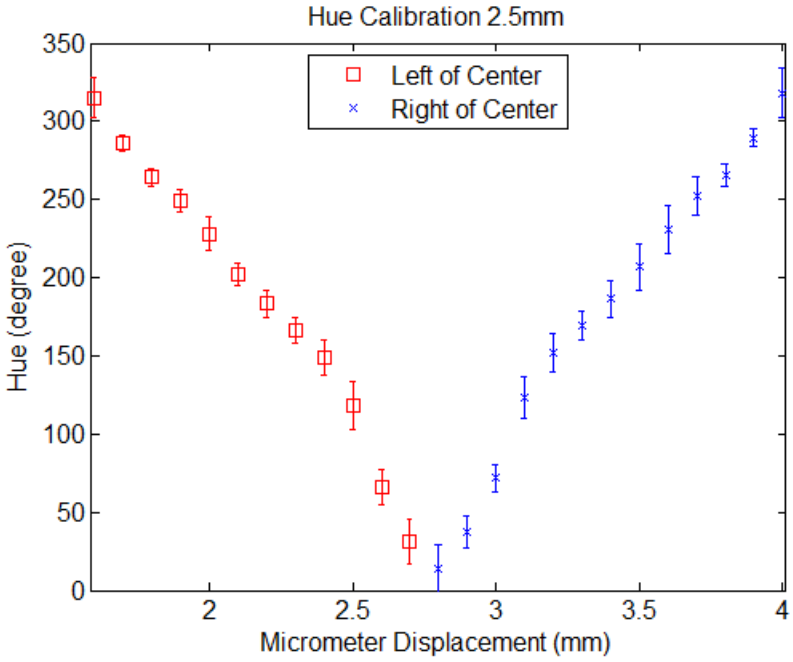
Hue Calibration 2.5mm
Left of Center
Right of Center
Hue (degree)
Micrometer Displacement (mm)
0
50
100
150
200
250
300
350
2
2.5
3
3.5
4

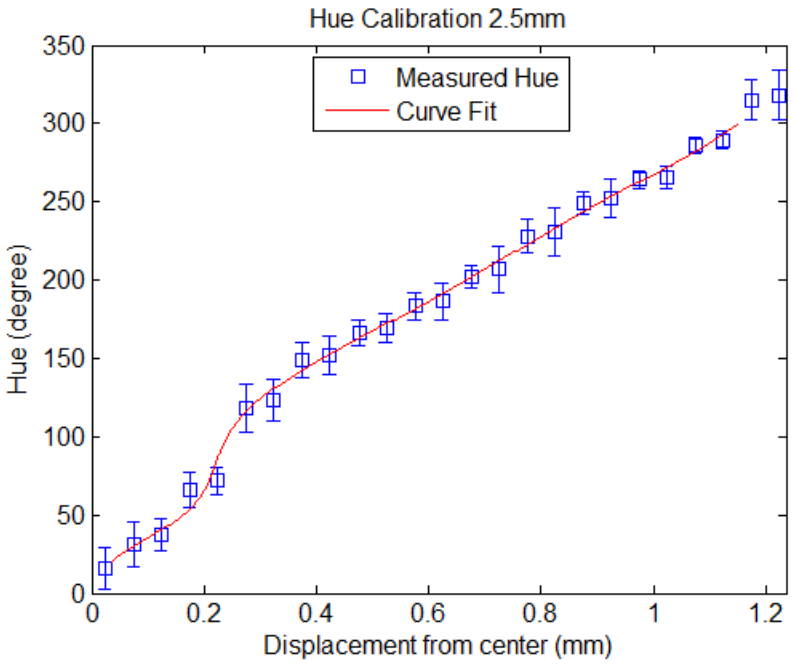
Hue Calibration 2.5mm
Measured Hue
Curve Fit
Hue (degree)
Displacement from center (mm)
0
50
100
150
200
250
300
350
0
0.2
0.4
0.6
0.8
1
1.2

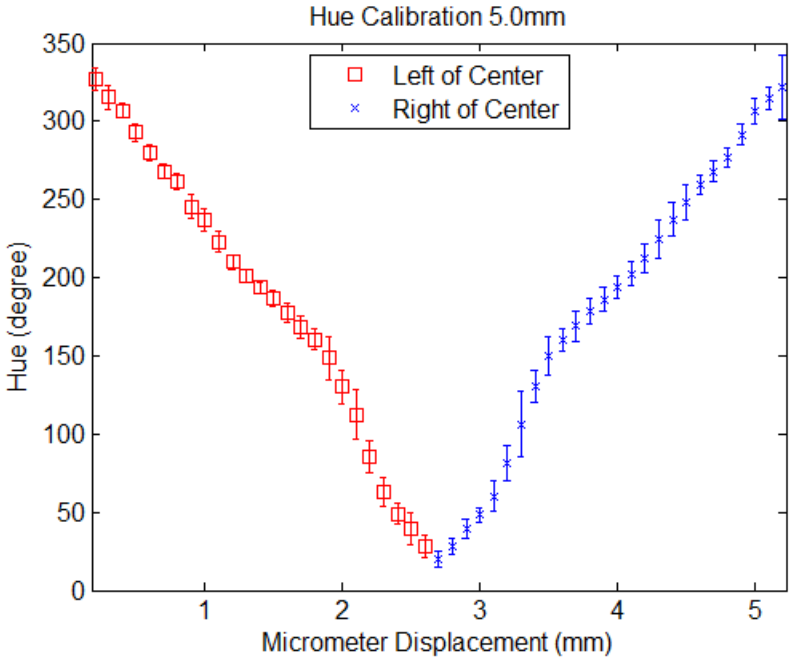
Hue Calibration 5.0mm
Left of Center
Right of Center
Hue (degree)
Micrometer Displacement (mm)
0
50
100
150
200
250
300
350
1
2
3
4
5

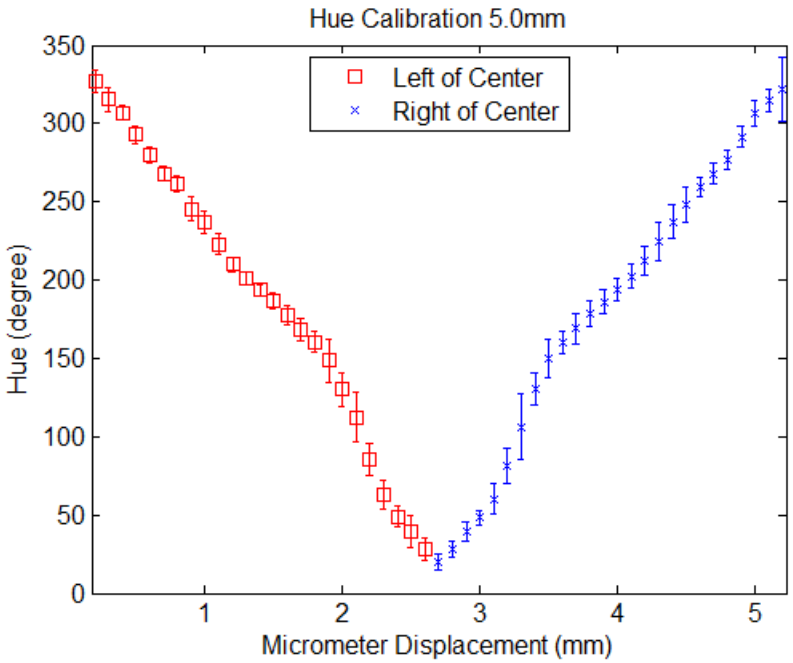
Hue Calibration 5.0mm
Left of Center
Right of Center
Hue (degree)
Micrometer Displacement (mm)
0
50
100
150
200
250
300
350
1
2
3
4
5